Engineering Structures 343 (2025) 120974

Contents lists available at ScienceDirect

Engineering Structures

journal homepage: www.elsevier.com/locate/engstruct

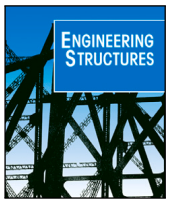

A novel methodology for structural health monitoring of buildings subjected to earthquakes

Sherif Beskhyroun *, Seyed Ehsan Aghakouchaki Hosseini

Department of Built Environment Engineering, School of Future Environments, Faculty of Design and Creative Technologies, Auckland University of Technology (AUT), 1010 Auckland, New Zealand

ARTICLE INFO

Keywords:
Structural health monitoring
Long-term monitoring
Damage detection
Damage progression
Adaptive time-series models

ABSTRACT

Recent advancements in sensor technology and data processing algorithms have revolutionized Structural Health Monitoring (SHM), enabling real-time monitoring and analysis of structural responses to dynamic loads. As a result, many buildings are permanently instrumented with sensors, typically accelerometers, to continuously record vibrational responses over time, hence generating huge amounts of monitoring data. However, the analysis and extraction of meaningful insights from the recorded data to assist engineers and building managers in assessing structural conditions would be a challenge. Monitoring systems can be programmed to record ground motion-induced vibrations that surpass specific trigger threshold levels. Nonetheless, there are challenges to long-term damage detection of buildings including automated analysis of previously recorded data, the limited number of available sensors, and nonlinear structural responses under severe earthquakes, to name but a few. In this paper, a new methodology based on adaptive time-series (TS) models for SHM and damage detection in buildings subjected to earthquakes is introduced to overcome these challenges. Using the proposed technique, automated analysis of a large set of previously recorded data and establishing a reliable baseline for the structure using a limited number of sensors, even as few as two accelerometers (one on the building and one on the ground) would be achievable. The efficiency of this method for monitoring large-scale structures instrumented with a limited number of sensors is verified using a 3-D Finite Element (FE) model of a 5-story reinforced concrete (RC) building using SAP2000 platform. Furthermore, experimental validations of the technique were implemented using acceleration datasets of a full-scale two-story post-tensioned concrete wall building tested over a shake table for damage assessments. The simulation results and experimental verifications demonstrated accurate identification of potential damage and provided a clear indication of damage progression as the severity of induced damage increases.

1. Introduction

Civil structures and infrastructures constitute the fundamental parts of various industries including transportation, buildings, and strategic industries, among many others. These structural systems are subject to a spectrum of degradation, deterioration, and damage scenarios under catastrophic natural hazards such as earthquakes, strong winds, floods, environmental corrosion, material aging, etc. Structural health monitoring (SHM) techniques are a substantial research topic with direct application in a variety of industries including civil structures and infrastructures such as buildings [1], bridges [2,3], fluid tanks [4], aerospace [5], mechanical systems [6], offshore jacket platforms [7], to mention but a few. In a general sense, these techniques can be applied to different purposes, including structural design validation, nonlinear response identification, diagnosis and prognosis of damage for maintenance aims, and rapid disaster management. Different types of sensors can be utilized for SHM purposes. These sensors can be categorized into three main groups, including kinematical, mechanical, and ambient sensors. Kinematical sensors comprise accelerometers [8], velocity sensors, and displacement sensors such as linear variable differential transformers (LVDT's) and laser displacement sensors [9]. In the group of mechanical sensors, one can mention load cells and strain gauges [10–12] while anemometers and thermocouples could be named for the class of ambient sensors. A series of novel sensors newly developed for SHM applications include fiber optic (FOS)-based sensors [8,13] such as fiber-brag-grating (FBG) sensors [14], piezoelectric and capacitive stress sensors [15], and vision-based sensors [16–18], among others. A comprehensive description of a variety of sensors

* Corresponding author.
E-mail addresses: sherif.beskhyroun@aut.ac.nz (S. Beskhyroun), ehsan.hosseini@autuni.ac.nz (S.E.A. Hosseini).

https://doi.org/10.1016/j.engstruct.2025.120974
Received 30 December 2024; Received in revised form 9 June 2025; Accepted 12 July 2025
Available online 28 July 2025

Nomenclature

ANN	Artificial Neural Network	HHT	Hilbert–Huang transform
AR	Autoregressive	LVDT	Linear variable differential transformer
ARIMA	Autoregressive integrated moving average	MA	Moving average
ARMA	Autoregressive moving average	ML	Machine learning
ARMAX	Autoregressive moving average with exogenous inputs	MUSIC	Multiple signal classification
ARX	Autoregression with exogenous inputs	NN	Neural networks
BPNN	Back propagation neural network	NRMSE	Normalized Root Mean Square Error
BP	Bayesian probabilistic	PEER	Pacific Earthquake Engineering Research Center
CNN	Convolutional Neural Network	PGA	Peak ground acceleration
DA	Domain Adaptation	RC	Reinforced Concrete
DFT	Discrete Fourier transform	RF	Random Forest
DI	Damage indicator	SHM	Structural health monitoring
DL	Deep learning	SVM	Support vector machine
FBG	Fiber-brag-grating	TL	Transfer Learning
FDD	Frequency domain decomposition	TS	Time series
FE	Finite Element	VAE	Variational Auto-encoder
FFNN	Feed Forward Neural Network	VAR	Vector autoregressive
FOS	Fiber optic-based sensor	VFP	vector-dependent functional pooled
FRF	Frequency response function	WT	Wavelet transform
FTS	Fit score	WVD	Wigner-Ville distribution

applied for SHM techniques can be found in [19]. Accelerometers are a group of low-cost, easy-installation sensors that are widely employed for long-term health monitoring applications [20].

Seismic SHM [21], specifically, focuses on the application of SHM procedures to earthquake engineering in which these techniques play a pivotal role in establishing a reliable procedure for long-term monitoring of structural systems over their lifetime. They particularly assist engineers in assessing the structural conditions and allow decision-makers to take appropriate post-disaster actions. Various SHM techniques have been proposed and examined in the literature for detection, localization, and quantification of structural damage and deterioration [22,23]. Approaches based on structural demand parameters including hysteretic energy and ductility, have been applied to the damage assessment of Reinforced Concrete (RC) structures [20,24,25]. Vibration-based approaches are among the most widely used methodologies for this aim [26–29]. These techniques rely on robust signal processing techniques [30] to identify changes in the vibrational responses of the structure that are transmitted through variations in the dynamic behavior and structural characteristics of the system such as stiffness [8,31–34]. Among various vibration-based SHM techniques, one can mention modal-based methods [35], Bayesian Probabilistic (BP) methods [36], time-series (TS) models, Wigner-Ville Distribution (WVD) [37], Wavelet Transform (WT) [38], Hilbert–Huang Transform (HHT) [39], FE model-updating [40], etc.

Generally, the applied SHM techniques are classified into two main groups, time-domain and frequency-domain approaches. Some of the applied techniques in frequency-domain include Discrete Fourier Transform (DFT) [41], Frequency Response Function (FRF) [42], Multiple Signal Classification (MUSIC) [43], and Frequency Domain Decomposition (FDD) [44] can be named. In frequency-domain or modal-based techniques, the changes in modal parameters such as natural frequencies, mode shapes, and damping ratios are utilized to detect the damage in the system [45]. When using frequency-domain signal processing methods, the localization and quantification of the damage could be a challenge [46,47]. On the other hand, the minimal changes in frequency resulting from damage are unlikely to be detectable by an SHM system, as such systems are generally not capable of determining frequency with the required high resolution. Furthermore, frequency variations due to seasonal temperature changes or electromagnetic noise in the recorded data typically exceed these minor changes. Although the methods in this group play a pivotal role in updating the structural model, their computational burden, modeling error, and uncertainties can lead to substantial variations in damage indicators [48–50]. The gap in FE model-updating methods can be reduced through conducting dynamics tests to reduce the modeling error and uncertainties, however, they cannot be removed totally, hence reducing the efficiency and performance of the technique.

In time-domain signal processing techniques, one can mention the statistical TS models for detecting the state of the system. These approaches have found applications in different fields such as system identification, structural dynamics, financial applications, social sciences, medicine, etc. [51]. The main advantage of data-based statistical TS methods is their robustness against signal faults and no requirements for visual inspection of the structural system in the process of damage detection [47] or physical models. These methods work based on a mathematical approximation of the system, which is built on the input signal and output measurements and could be modeled using a linear or nonlinear model. Among statistical TS-based methods one can mention Autoregressive (AR) model [1,52], Moving Average (MA) [53], Autoregressive Moving Average (ARMA) [54], Vector Autoregressive (VAR) [55], Auto-Regressive with eXogenous inputs (ARX) [56–58] which has proved efficient and successful applications for TS modeling of data in the field of SHM and damage detection [57,59], Autoregressive Moving Average with Exogenous inputs (ARMAX) [60,61], a method based on a combination of AR with ARX termed as ARARX [62], an ARX model based on vector-dependent functional pooled model (VFP) named VFPARX [63]. However, the performance of these methods may degrade under non-stationary conditions such as seismic events, rapidly changing dynamics, and nonlinearities [64]. Efforts have been made to handle such issues by introducing time-varying (TV) time-series techniques such as TV-AR [65], TV-ARMA [66], Autoregressive Integrated Moving Average (ARIMA) [67,68], among others. Nevertheless, the sensor placement effect on the damage localization, which adversely affects the accuracy of these

methods, priori knowledge of the system dynamics, sensitivity to noise, and computational burden remain concerning issues for such strategies [64,69–71]. As sensors applied for SHM purposes generate huge amounts of recorded data over years of monitoring, it becomes increasingly challenging to analyze and extract meaningful insights to assess structural conditions. Automated analysis of previously recorded monitoring data to establish reliable baseline performance features that can be used for damage detection and accurate condition assessment is both challenging and crucial for the successful implementation of long-term monitoring of buildings. Additional typical challenges in the long-term monitoring of large-scale structures include the limited number of available sensors and the nonlinear response of structures to large-magnitude earthquakes. Acquiring such insights will become particularly important following earthquakes, and throughout a building's life cycle, when damage may occur due to aging and fatigue.

A variety of machine learning (ML) approaches have been proposed in the literature for structural damage detection. A series of these techniques was developed to reduce the adverse effects of uncertainties and modeling errors in vibration-based model-dependent SHM methodologies. Chun et al. 2015 [72] proposed a probabilistic method based on multi-point acceleration measurement and Artificial Neural Networks (ANN) to quantify the severity of the damage and determine its location. Rafiei and Adeli, 2018 [73] developed an unsupervised Deep Learning (DL) technique for feature extraction from the frequency domain of the recorded signals. Ma et al. 2020 [74] presented a method based on Variational Auto-encoder (VAE) for unsupervised feature extraction. Transfer learning (TL) approach, a branch of ML that uses knowledge from different domains (target and source) and Domain Adaptation (DA) technology, has recently shown successful applications for structural damage identification [50,75–77] by bridging the gap between model-based SHM techniques and real applications. Other methods such as Convolutional Neural Networks (CNNs) [78,79], Feed Forward Neural Networks (FFNNs) [80], Back Propagation Neural Networks (BPNNs) [81], an image-based technique using DL and Bayesian optimization [82], Support Vector Machine (SVM) [83], and Random Forest (RF) [84], among others, have been applied for the detection of damage in structures. A series of review studies conducted on different ML techniques applied to SHM and damage detection of civil structures can be found in [85–87]. However, even though data-driven methods have proved efficient and powerful in seismic damage detection, simulating uncertainties under different mechanisms and patterns, environmental complexities, large and labeled dataset requirements, and additional bias in the case of probabilistic methods may pose constraints in front of these techniques and make them suffer from poor generalizability across structures and seismic intensities.

In this research, as a step forward in addressing some of the challenges that face the described seismic SHM techniques and removing the current gaps, a vibration-based data-dependent methodology based on a novel adaptive ARX technique has been proposed. The proposed technique is not computationally intensive and has proved efficient in tackling challenges such as handling nonlinearities under different seismic intensities and PGA levels, the sensor placement effect on the damage localization and the effect of the number of sensors, and flexibility and practicality for real-time applications on full-scale buildings. The proposed method is able to provide clear indications of damage under different scenarios, thereby demonstrating both the robustness of the method and its capability to detect low levels of damage using only a minimal sensor configuration. The key advantages of the proposed methodology can be listed as follows,

- **Minimal sensor requirements:** The method can be applied with a minimal number of sensors (at least two: one for building response and one for ground motion), making it practical for various structures.
- **Utilization of historical data:** By using historical earthquake responses to create baseline models, the method improves its predictive capability as the number of available recorded earthquakes increases. This results in better simulation of new earthquakes and more accurate anomaly detection.
- **Handling nonlinear responses:** The method is adaptable for linear TS models (such as ARX) to model bilinear or trilinear responses. By classifying building responses according to PGA and calculating baseline models for each class independently, the method can handle changes in stiffness or dynamic characteristics during medium and high magnitude earthquakes.
- **Flexibility and verification:** Other time series models can be implemented within the same methodology, allowing for comparison and further verification of results.
- **Practicality and real-time implementation:** The method is practical and can be easily implemented in structures permanently instrumented in seismically active regions. It also supports automatic and real-time operation, enhancing its utility for continuous monitoring and immediate damage detection.

To evaluate the efficacy of the proposed technique, validation was conducted using a three-dimensional SAP2000 model for a 5-story reinforced concrete (RC) building and the time–history responses at key locations of the structure were extracted for analyses. The case study was developed to demonstrate the practical applicability of the proposed procedure for assessing the condition of multi-story buildings subjected to ground motion using a very limited number of sensors. To substantiate the efficacy of the proposed approach, numerical models were employed wherein damage levels were introduced in such a way as to yield only a very slight change in the natural frequency — changes that would typically be challenging to detect with conventional damage identification techniques. Moreover, the method was further validated against bidirectional shake table tests' results of a two-story full-scale post-tensioned concrete wall building. Various damage scenarios in terms of damage sizes and diverse damage types were investigated. The results demonstrated the robustness of the proposed method to sensor proximity and its efficiency in handling nonlinearities through classifying the response signal into separate regions of different PGA levels, detecting damage in real-time, quantifying damage, localizing damage, and indicating its progression across various sizes, types, and locations, despite the deployment of only a minimal number of sensors far from the damage location. It is also important to note that, for the case of numerical simulations, the applied ground motions were characterized by high randomness and complexity. The fact that the method without utilizing a complicated and computationally intensive algorithm successfully identified low levels of damage under these conditions–using merely two sensors–underscores the novelty, performance, and practical value of the approach in real-world seismic structural health monitoring applications.

2. Methodology

The proposed methodology for structural health monitoring and damage detection is designed to work with a structure instrumented with accelerometers at various locations, along with a free-field accelerometer to record ground motion during earthquakes. The flowchart of the proposed technique has been indicated in Fig. 1.

The proposed approach involves the following key steps:

I. **Model creation and classification**

a. **Time series mathematical model:** For each measuring sensor in the building, a time series mathematical model is created using the ground motion as the input and the building response at a specific location as the output.

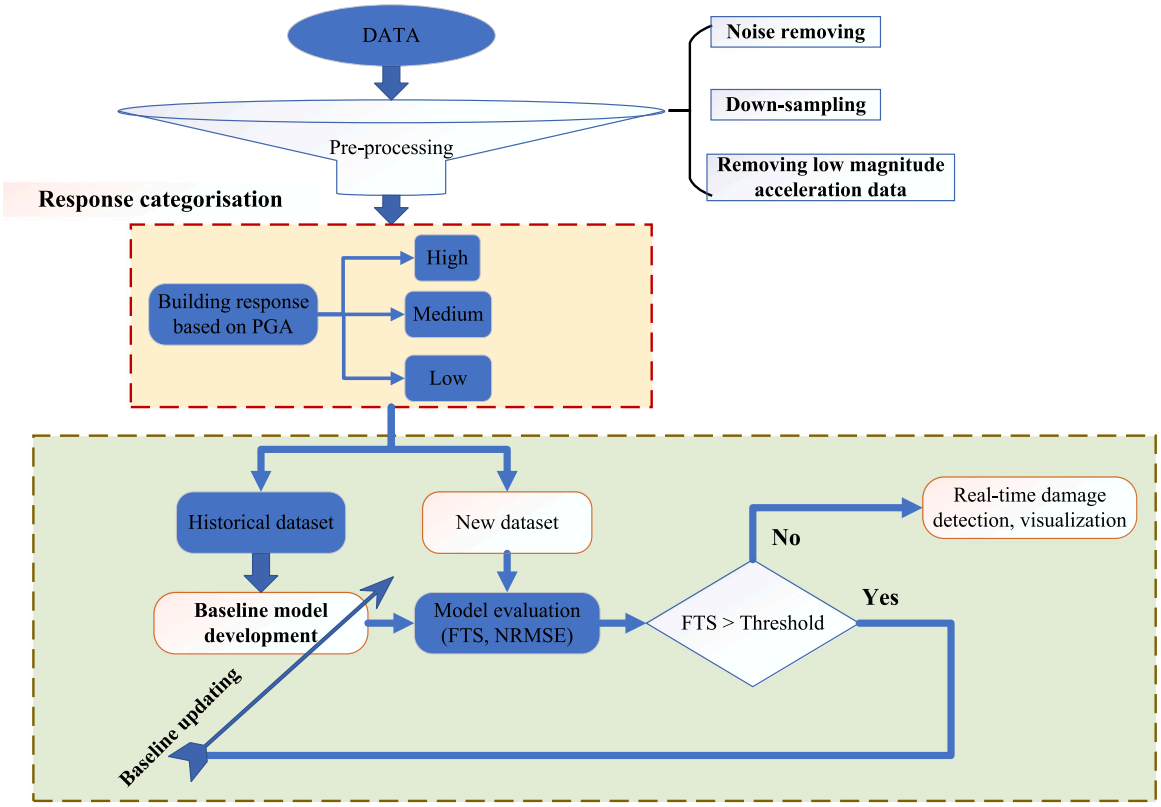

Fig. 1. Proposed automated real-time SHM and damage detention technique.

b. **Nonlinear response classification:** To account for possible nonlinear behavior (assuming bi-linear or tri-linear models), the building's response is classified based on the peak ground acceleration (PGA) into high, medium, and low categories. The classification thresholds for PGA are determined by the user according to the building's performance criteria. In this study, the peak ground acceleration (PGA) threshold is set to a high value so that all available data sets are classified in one category (for example, Low PGA). The methodology presented in this research is inherently scalable and adaptable. In scenarios where a more extensive dataset is available–encompassing a sufficiently large number of ground motions across diverse PGA ranges (e.g., Low, Medium, High)–the framework can systematically be extended to incorporate multi-level PGA classifications.

c. **Independent models for each sensor:** For each sensor in the building, an independent model is created using the building's response to a single ground motion excitation.

II. **Baseline model development**

i. **Use of historical data:** Historical earthquake response data collected during the monitoring period are used to calculate baseline models for future assessments. For each recorded earthquake response, independent models are created for each sensor using the ground motion as input and the sensor response as output.

ii. **Number of baseline models:** The number of baseline models equals the number of sensors multiplied by the number of recorded earthquake responses.

iii. **Fit score and residual error calculation:** For each baseline model, the fit score and residual error between the predicted response by the model and the actual measured response are calculated. Threshold limits for these metrics are established based on the baseline models. For example, the minimum fit score among all baseline models for a specific sensor is used as the threshold limit for the fit score, and the maximum residual error is used as the threshold limit for the residual error.

III. **Application to new earthquake data**

A. **Assessment of new earthquake responses:** When a new earthquake occurs, the recorded ground motion is used as input to the baseline models to predict the building's response. The predicted response and the actual measured response are compared to evaluate the fit score and residual error against the established thresholds. As seen in the technique's flowchart in Fig. 1, for a new dataset (ground motion), if the condition $FTS > Threshold$ is true, the dataset is added to the historical dataset, and the baseline model is updated.

B. **Damage detection:** If the fit score or residual error for the new earthquake response falls below the threshold limit, it indicates potential damage. The building managers are then notified of the possible damage.

By following this methodology, building managers can ensure continuous monitoring and timely detection of structural damage, improving the overall safety and resilience of civil infrastructure. Details of the proposed method are described in the following key sections.

2.1. Data preprocessing

Noisy and low magnitude acceleration data near the end of the building response that is below a specific acceleration value is discarded to minimize the effect of noise and to enhance the model fitting.

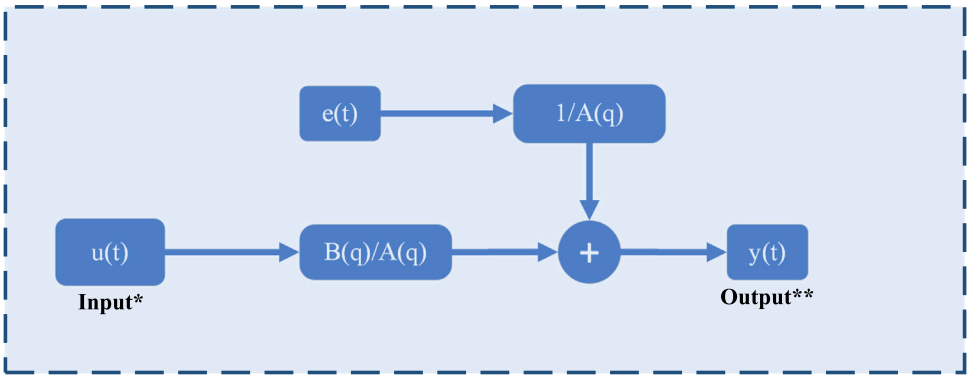

*** Input data from the free-field accelerometer sensor at the ground level close to the building**

**** Output data from accelerometer sensor attached to the building**

Fig. 2. Block diagram of the ARX model structure.

The acceleration data is then down-sampled to reduce the size of the data and to remove the unwanted high-frequency components of the data, as buildings' natural frequencies are typically lower than most of the SHM systems' sampling frequencies. This procedure reduces computational load and discards insignificant data points, focusing on the critical portions of the signals.

2.2. Categorization of the structural responses

The structure's responses are categorized based on the PGA to High, Medium, and Low classes before fitting the time series models. This categorization is carried out to account for the possible nonlinear, bilinear or trilinear response of the structure during high-magnitude earthquake shaking. The maximum absolute ground acceleration is used to categorize the data into high, medium, or low levels. This categorization is crucial as it is invaluable to develop different models for each response level to capture the corresponding structure's modal characteristics during this particular level of shaking. Fitting a linear model that can represent the structure that behaves nonlinearly or experiences a shift in stiffness during large magnitude shaking is not possible and can lead to incorrect prediction of the response and consequently decrease the accuracy of assessing the structure's conditions.

2.3. Baseline ARX model development

Once the structure's response is pre-processed and categorized as outlined in the previous stages, the data is normalized with respect to the maximum of the absolute value of the data. Then, an ARX model is calculated using the ground motion data as the input $u(t)$, sensor response as the $y(t)$, and the model prediction error $e(t)$. Fig. 2 depicts the ARX model structure block diagram.

The structure of the ARX model is formulated as follows,

$$A(q)y(t) = B(q)u(t - n_k) + e(t) \tag{1}$$

$$A(q) = 1 + a_1 q^{-1} + \cdots + a_{n_a} q^{-n_a} \tag{2}$$

$$B(q) = b_1 + b_2 q^{-1} + \cdots + b_{n_b} q^{-n_b+1} \tag{3}$$

where the q in the above equations is the delay operator. Eq. (1) can be expanded as follows,

$$y_i(t) = \sum_{j=1}^{n_a} a_j y_j(t - j) + \sum_{k=1}^{n_b} b_k u(t - k) + e(t) \tag{4}$$

where $y_i(t)$ is the structure's response at time t, $u(t)$ is the ground motion, n_a and n_b are the ARX model orders and k is the delay between input and output. a_j and b_k are the model coefficients and $e(t)$ is the error term.

2.4. Model evaluation

The performance of each ARX model is evaluated using the fit score (FTS) and Normalized root mean square error (NRMSE), as defined below,

$$FTS = 100 \times \left(1 - \frac{\|y - \hat{y}\|}{\|y - \bar{y}\|}\right) \tag{5}$$

$$NRMSE = \frac{\sqrt{\frac{1}{N}\sum_{i=1}^{N}(y_i - \hat{y}_i)^2}}{max(y) - min(y)} \tag{6}$$

where y, $\hat{y}$, $\bar{y}$, y_i, $\hat{y}_i$, N, $max(y)$, $min(y)$, are the vector of the actual output data, the vector of predicted output data from the ARX model, the mean of the actual output data, actual output at time i, predicted output at time i, the number of data points, and the maximum and minimum values of the actual output, respectively. The $\|.\|$ operator represents the Euclidean (L_2) norm. For each sensor data (L), data file (M), and PGA category (C), an ARX_{LM}^{C} and the corresponding FTS_{LM}^{C} and $NRMSE_{LM}^{C}$ are calculated. This process is repeated automatically using all available earthquake responses that had been recorded by the monitoring system in the past. The calculated ARX models, FTS, and NRMSE will be used as baseline models and parameters for evaluating the structure's response due to future measured earthquakes and assessing its conditions. To ensure a high quality of the baseline models, ARX models with FTS below a specific value can be discarded. As many structures have been monitored for several years, previously recorded earthquake responses with various magnitudes can be available. Hence, baseline ARX models that represent the structure's performance due to various ground motions can be made available using the available data. Therefore, the ability of the developed ARX baseline models to predict the structure's response due to future earthquakes and hence assess its condition can be enhanced significantly. Fig. 3 concisely presents the structure of the proposed methodology for developing the ARX models for N number of datasets from different available ground motions ($\ddot{u}_{g1}.....\ddot{u}_{gN}$) and the corresponding building's acceleration measurements ($a_1.....a_N$) provided by a sensor connected to it. The developed models are then employed for damage assessment at a certain damage level by inputting any given ground excitations to predict the structure's accelerations ($\hat{a}_1.....\hat{a}_N$), obtain the best FTS and the minimum NRMSE, and finally, damage quantification and localization, and determining damage progression will be indicated.

2.5. Real-time damage detection

Once the baselines have been calculated, the newly measured earthquake response can be analyzed. Previous steps involving data truncation, down-sampling, and categorization, are carried out on the

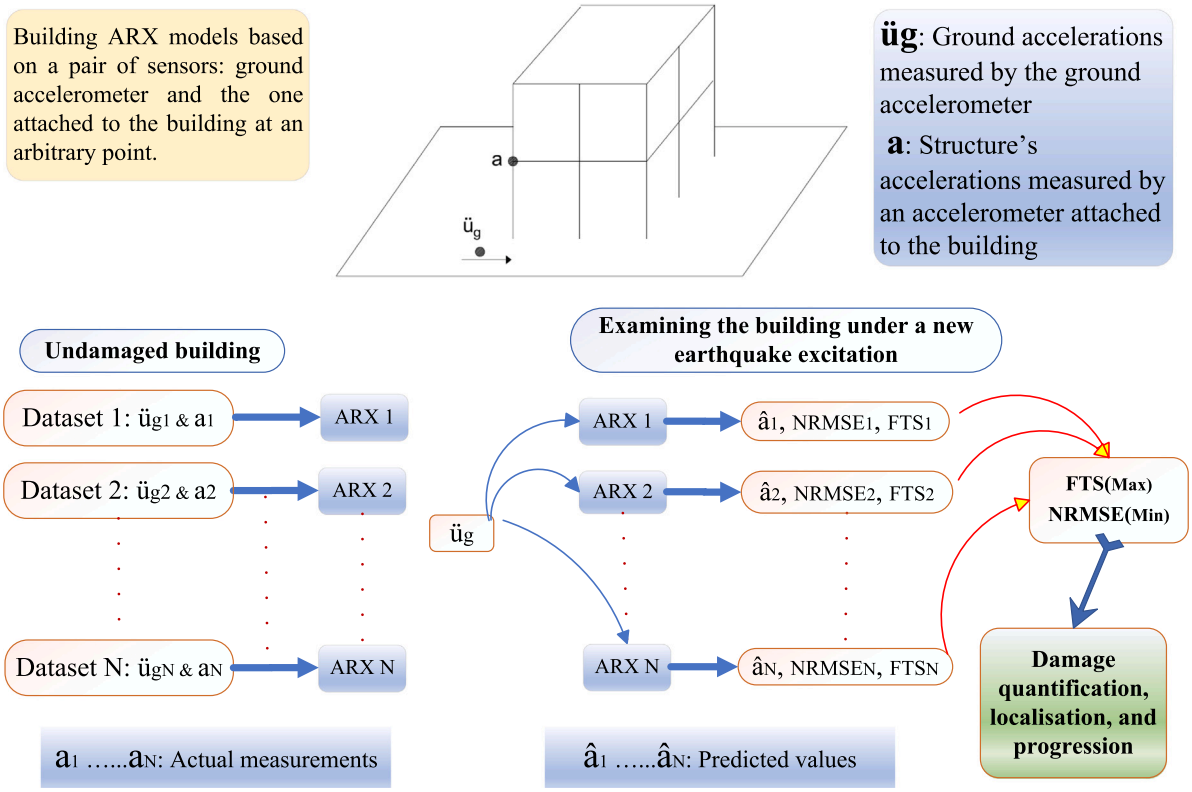

Fig. 3. Schematic of the methodology for developing the ARX models and acquiring the best FTS and minimum NRMSE.

new dataset. The processed ground motion is then used to predict the structure's response at each measuring sensor using all available baseline ARX models under the corresponding PGA category (High, Medium, or Low). For each available ARX baseline model, the FTS and NRMSE values are calculated using the predicted response from the ARX model and the actual response measured by the actual sensor. The number of calculated FTS and NRMSE values is equal to the number of baseline models under the ground motion category. The best baseline ARX model that can predict the structure's response due to the newly measured earthquake will provide the maximum FTS value and the minimum NRMSE. Hence, the maximum FTS and the minimum NRMSE for each measuring sensor are determined for the newly measured earthquake response. The FTS and NRMSE can then be compared to the predetermined threshold values for damage detection. A damage indicator (DI) is defined as below,

$$DI = FTS_{udm} - FTS_{dm} \tag{7}$$

where, the FTS_{udm} and FTS_{dm} are the fit scores in two states of undamaged and damaged, respectively. In case of damage detection, the values of FTS and NRMSE are recorded for evaluating the structure's response afterward to determine if there is a further drop in the FTS and a further increase in the NRMSE to monitor any potential growth in the damage level and further deterioration in the structure's condition.

2.6. Adaptive baseline update

Continuously updating the baseline models with new earthquake data that fits well, ensuring the SHM system remains accurate and reflective of the current structural state. If the fit scores for the new data exceed specified thresholds, indicating normal structural conditions, new ARX models are fitted and added to the existing collection. This continuous update ensures the predictive models remain accurate and reflective of the current structural state. Visualizations, including 3D bar plots of residuals, NRMSE, and fit scores, are generated to provide a comprehensive assessment of the new data in relation to the pre-existing models.

3. Results

3.1. Numerical evaluations

A 5-story RC building was modeled in SAP2000 as shown in Fig. 4 for conducting analytical simulations and investigating the performance and efficiency of the proposed SHM and damage detection technique. The beams' depths and widths were considered as 500 mm and 400 mm, respectively. The cross section dimensions of columns were regarded as 500 mm by 500 mm. The slab thickness in all floors was considered as 300 mm defined as shell elements. The material properties of the concrete including the density of 23.5 kN/m^3 and modulus of elasticity $E = 30$ GPa were considered for analyses. A number of 20 ground motions (RSN1–RSN20) were downloaded from the Pacific Earthquake Engineering Research Center (PEER), Next Generation Attenuation (NGA-West2) database for historical earthquake records [88], (https://ngawest2.berkeley.edu/). These records were used to develop the baseline ARX models for the undamaged building. In contrast, other ground motions including RSN21 and RSN25 which were not included in the baseline model development, were used to simulate a case where the ground motion characteristics differ significantly, thereby testing the robustness of the damage identification method under unfamiliar seismic inputs. Each floor was instrumented with a single accelerometer positioned at the intersection of columns with beams on the gridline 1-A as illustrated in Fig. 4. For validation purposes, only a small subset of ground motion records was applied in a linear dynamic time–history analysis. Each ground motion excitation was set up manually within SAP2000, and time–history responses were extracted at five key locations in the structure for each excitation. The acceleration time–history responses are measured at five locations along the height of the columns at the gridlines 1-A, on floors 1–5 of the RC building under different damage scenarios to examine the efficiency and performance of the developed damage detection technique. The validation process involved performing a comprehensive time history

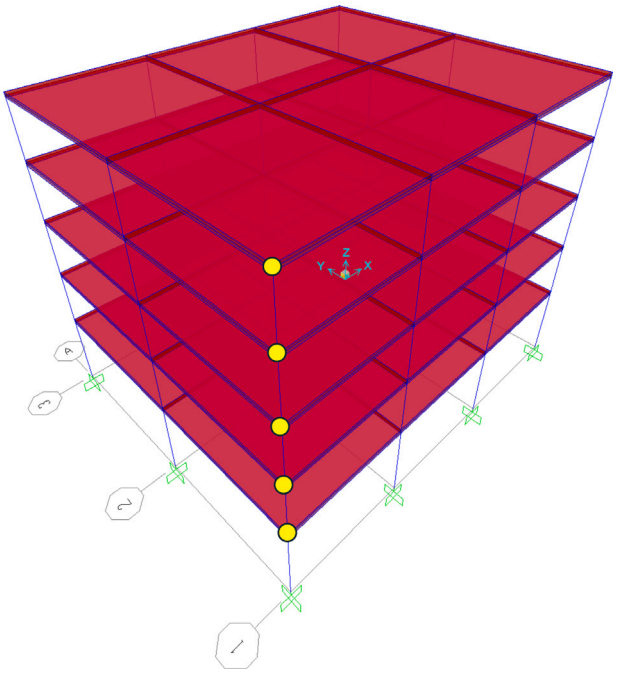

Fig. 4. 3D FE model of the 5-story RC building instrumented with accelerometer sensors over gridline 1–A on all stories, modeled in SAP2000.

Table 1
Frequency shift due to various damage scenarios at different damage levels calculated using modal analysis based on FE model of the building in SAP2000.

Damage case	F_Y (Hz)	F_X (Hz)	$(F_Y^{udm} - F_Y^{dm})$ (Hz)	$(F_X^{udm} - F_X^{dm})$ (Hz)
Undamaged	0.57073	0.63228	–	–
Damage case I				
Damage level 1	0.57021	0.63167	0.00052	0.00061
Damage level 2	0.56968	0.63091	0.00105	0.00137
Damage level 3	0.56915	0.63013	0.00158	0.00215
Damage case II				
Damage level 1	0.56966	0.63103	0.00107	0.00125
Damage level 2	0.56857	0.62943	0.00126	0.00285
Damage level 3	0.56749	0.6277	0.00324	0.00458
Damage case III				
Damage level 1	0.5688	0.63006	0.00193	0.00222
Damage level 2	0.56782	0.62894	0.00291	0.00334
Damage level 3	0.56723	0.62826	0.0035	0.00402

analysis to simulate acceleration responses induced by ground motion excitations. Modal analysis was conducted to calculate the acceleration time history response from the ground motion excitations. A constant damping ratio of 5% was applied for all modes.

3.2. Defining damage scenarios

In this section, three main damage cases (I–III) are introduced to evaluate the performance of the proposed technique in structural damage identification and localization in the considered RC building model. These damage cases were examined under ground motions RSN14 and RSN21. The former ground motion was included in the development of the designed ARX model while the latter was not included. An additional damage scenario at three cases and three damage levels each was examined which results thereof can be found in Appendix. Detailed descriptions of these damage scenarios and cases, and the obtained results are discussed in the next sections.

Table 2
FTS_{max} and $NRMSE_{min}$ values under different damage cases and levels for each sensor.

Damage Case	Damage level	FTS_{max} (%)	$NRMSE_{min}$
Sensor 1 at 1st floor			
Damage Case I	1	96.93	0.237
	2	95.23	0.364
	3	93.40	0.50
Damage Case II	1	94.83	0.904
	2	93.46	1.075
	3	91.24	1.377
Damage Case III	1	94.57	0.953
	2	93.86	1.044
	3	93.35	1.110
Sensor 2 at 2nd floor			
Damage Case I	1	97.65	0.152
	2	95.93	0.261
	3	93.96	0.386
Damage Case II	1	96.97	0.451
	2	94.67	0.736
	3	91.86	1.096
Damage Case III	1	96.28	0.527
	2	95.09	0.669
	3	94.35	0.759
Sensor 3 at 3rd floor			
Damage Case I	1	97.45	0.174
	2	95.18	0.338
	3	92.71	0.522
Damage Case II	1	96.46	0.569
	2	93.83	0.904
	3	90.78	1.323
Damage Case III	1	95.99	0.622
	2	94.72	0.773
	3	93.93	0.870
Sensor 4 at 4th floor			
Damage Case I	1	97.85	0.123
	2	95.97	0.232
	3	93.93	0.352
Damage Case II	1	94.44	1.270
	2	91.51	1.901
	3	88.17	2.661
Damage Case III	1	94.59	1.187
	2	93.38	1.407
	3	92.60	1.553
Sensor 5 at 5th floor			
Damage Case I	1	97.97	0.080
	2	95.96	0.161
	3	93.82	0.250
Damage Case II	1	90.23	2.468
	2	88.43	2.840
	3	85.75	3.405
Damage Case III	1	88.35	2.812
	2	86.87	2.960
	3	86.49	2.996

3.2.1. Damage cases I and II; low-level damage

Two damage cases are defined based on reducing the modulus of elasticity of concrete, E_c, to specific percentage points for certain columns at the ground level on specified gridlines of the structure to simulate different damage levels. For damage case I, 10% reduction in E_c is introduced as below,

- **Damage case I - damage level 1:** 10% reduction in E_c for the column at gridline 1-A at the ground level only.
- **Damage case I - damage level 2:** 10% reduction in E_c for columns at gridlines 1-A and 1-B at the ground level only.
- **Damage case I - damage level 3:** 10% reduction in E_c for columns at gridlines 1-A, 1-B, and 1-C at the ground level only.

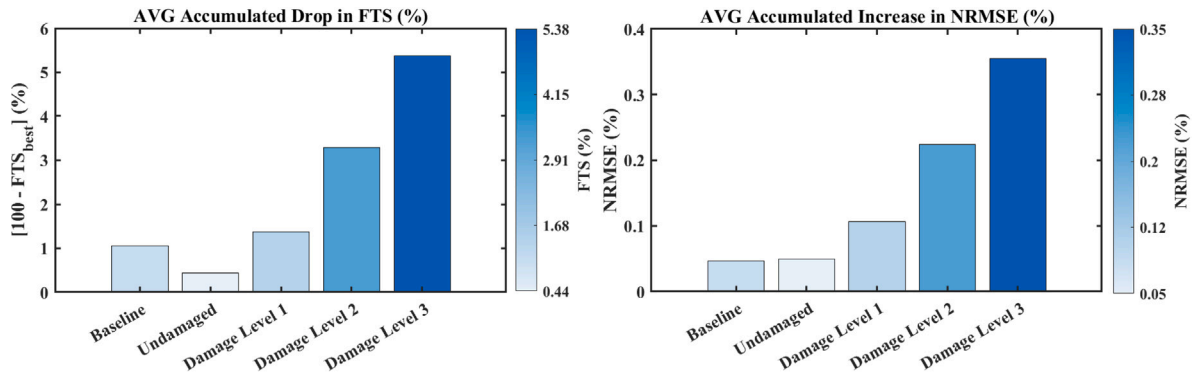

(a) Averaged accumulated drop in FTS (b) Averaged accumulated increase in NRMSE

Fig. 5. Average accumulated drop in FTS and increase in NRMSE for damage case I for the 5–story RC building under the ground motion RSN14; AVG: Average.

while for damage case II, 20% reduction in E_c is introduced as follows,

- **Damage case II - damage level 1:** 20% reduction in E_c for the column at gridline 1-A at the ground level only.
- **Damage case II - damage level 2:** 20% reduction in E_c for columns at gridlines 1-A and 1-B at the ground level only.
- **Damage case II - damage level 3:** 20% reduction in E_c for columns at gridlines 1-A, 1-B, and 1-C at the ground level only.

3.2.2. Damage case III; simulating a crack

In another scenario, a third damage case is introduced to simulate a crack in some locations in specified columns in the building. In fact, this damage case is introduced by localized reduction of E_c by 90% in specific segment lengths in these columns to examine the performance of the proposed methodology in damage localization in the building structure. This damage case is defined as below,

- **Damage case III - damage level 1:** reducing E_c in a 10 cm segment of the column at gridline 3-D at the ground level only.
- **Damage case III - damage level 2:** reducing E_c in a 20 cm segment of the column at gridline 3-D at the ground level only.
- **Damage case III - damage level 3:** reducing E_c in a 30 cm segment of the column at gridline 3-D at the ground level only.

3.3. Performance evaluation for introduced damages

To evaluate the performance of the proposed technique for damage identification and localization, the frequency shifts in the fundamental natural frequencies of the structural system are calculated for each damage case at different damage levels. It is worth noting that the change in frequency due to these various damage levels is very small, as shown in Table 1. In this table, F_X, F_Y, F_X^{udm}, F_Y^{udm}, F_X^{dm}, F_Y^{dm}, $F_X^{udm} - F_X^{dm}$, and $F_X^{udm} - F_X^{dm}$ are the fundamental natural frequencies of the structural system in the X and Y directions, the natural frequencies of the undamaged and damaged system in these directions, and the differences between the frequencies of undamaged and damaged system in these direction, respectively. As obvious from this table, by introducing different damage cases and damage levels 1–3, the frequency shift calculated from modal analysis using SAP2000 is in the range of 0.00052–0.00458 Hz which is considerably small. Such small changes cannot be detected in damage identification techniques based on frequency shifts as a result of damage scenarios in a structural system.

Figs. 5(a), 8(a), and 11(a) illustrate the average accumulated drop in FTS values for the defined damage cases for all three damage levels as well as the baseline and undamaged cases. The average accumulated increases in the NRMSE for the same damage cases and levels have been shown in Figs. 5(b), 8(b), and 11(b). For each damage case and a specific damage level, the FTS and NRMSE values are determined for each sensor based on its ARX model for each ground motion and then the average accumulated values of the drop in the former or increase in the latter are calculated based on the results of all sensors. The FTS_{best} in these figures is the best FTS value for each ground motion for all 5 ARX models of the 5 sensors at each specific damage level.

The maximum FTS and the minimum NRMSE values and their differences with the baseline have been depicted in Figs. 6–7, 9–10, and 12–13. In these figures,

$$FTS_{diff} = FTS_{max} - Baseline \tag{8}$$

$$NRMSE_{diff} = NRMSE_{min} - Baseline \tag{9}$$

A comparison between the maximum FTS and the minimum NRMSE values at different damage levels for each damage case, shown by FTS_{max} and $NRMSE_{min}$, has been presented in Table 2.

Moreover, for each damage case, with the progression of damage, meaning from damage level 1 to 3, the FTS values decrease and NRMSE values increase. This means that the method is sensitive enough to detect damage progression. When using a different ground motion, as in damage cases II and III, the calculated values of FTS and NRMSE change, but still in the close neighborhood of the other ground motion at similar damage levels for all sensors. This shows that the method can handle changes in ground motion characteristics and maintain its robustness, performance, and sensitivity for damage detection and progression. The results showed similar performance levels for all sensors in corresponding damage cases. For each damage case, the FTS_{max} and $NRMSE_{min}$ values for all sensors at different damage levels are close to each other. This demonstrates that the method has the capability to work based on only 2 sensors; one free-field sensor at the ground level for sensing ground motions as input and one sensor connected to the building for measuring the accelerations of the building as the output.

3.4. Examining high-level damage, sensor proximity, ground motion characteristics, and damage in other stories

Additional examinations were conducted for high-level damage, sensor proximity, and ground motion characteristics over the performance of the proposed technique for structural damage identification. The results of these analyses can be found in Appendix. Fig. A.23 illustrates the schematic of instrumentation and the selected columns at specified gridlines to define additional damage cases. Considering the results of Figs. A.24–A.27 for FTS and NRMSE for examining the effects of the sensor proximity on the results of damage detection shows very close values for each damage level in two damage cases IV and V which shows the robustness of the proposed technique in

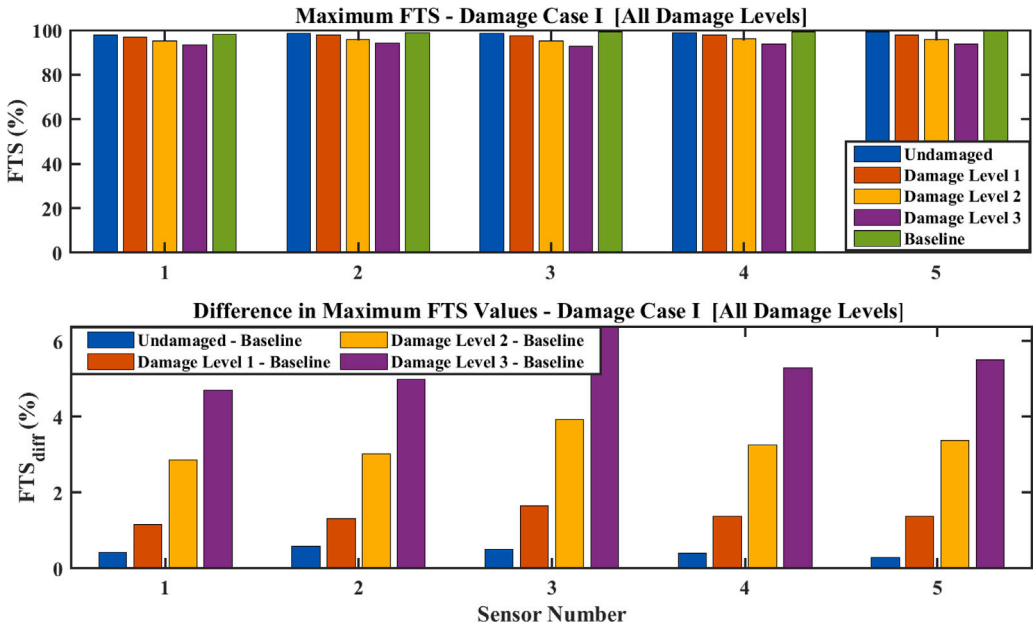

Fig. 6. Maximum FTS values and the difference between these values and the baseline, FTS_{diff}, for different damage levels at the location of each sensor for the 5-story RC building for damage case I under the ground motion RSN14.

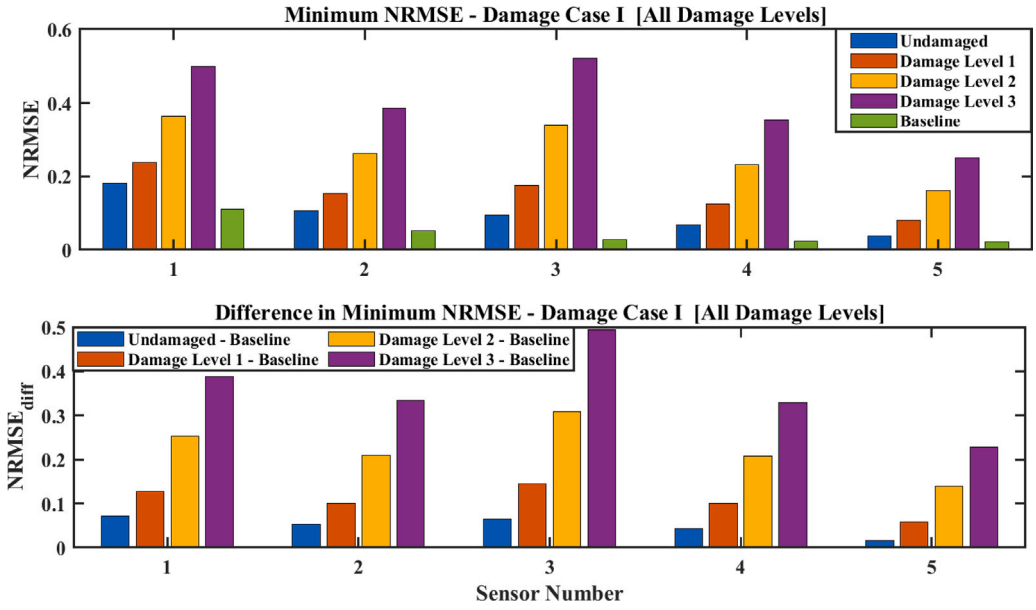

Fig. 7. Minimum NRMSE values and the difference between these values and the baseline, $NRMSE_{diff}$, for different damage levels at the location of each sensor for the 5-story RC building for damage case I under ground motion RNS14.

damage detection in terms of proximity of the damage location to the instrumented location (gridline 1-A) in the building. By changing the ground motion to RSN25 in damage case III and examining the results reflected in Figs. A.28–A.29 tangible changes in the calculated values of FTS and NRMSE compared to damage cases IV and V are observed which demonstrates the low sensitivity of the method to changes in the ground motion characteristics in damage detection. To further evaluate the performance of the technique in terms of the damage location, a new damage case (VII) as described in the Appendix was introduced. Figs. A.30–A.31 show the FTS and NRMSE values for each sensor at different damage levels for this damage case. The comparison of the FTS_{max} and $NRMSE_{min}$ values in these figures at each damage level for each sensor shows that these values are very close to each other. This demonstrates that the method is robust to sensor proximity and even in cases where sensors are far from the damage location, the method can still detect the damage with almost the same level of performance.

3.5. Experimental validation

In this section, the proposed methodology is validated using an available open-source dataset for damage assessment. The test structure is a full-scale post-tensioned concrete wall building. The test building was a two-story building of 4 m height at each story and plan dimensions of 5.4×8.95 m, weighted around 1350 kN and was designed using a direct displacement-based design method and was tested by Lu et al. 2021 [89]. The open-source dataset have been archived in DesignSafe-CI (http://www.designsafe-ci.org). This building was instrumented by

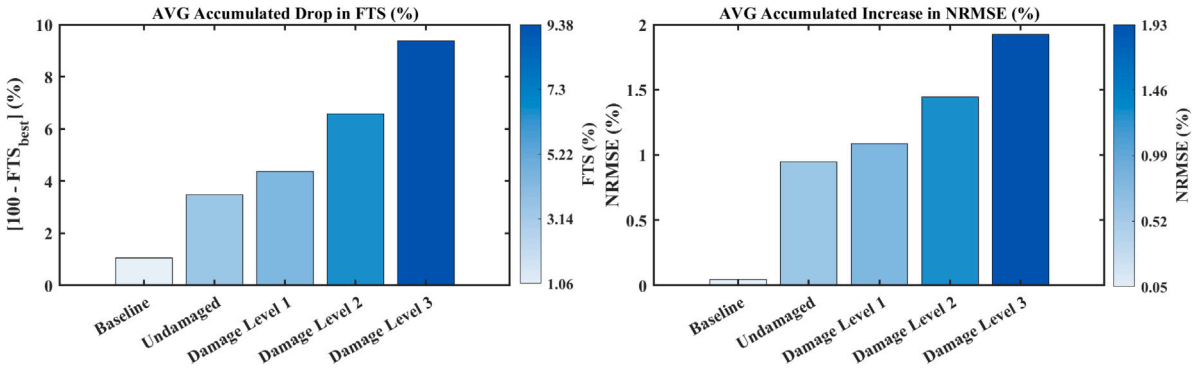

(a) Averaged accumulated drop in FTS (b) Averaged accumulated increase in NRMSE

Fig. 8. Average accumulated drop in FTS and increase in NRMSE for damage case II for the 5–story RC building under the ground motion RSN21; AVG: Average.

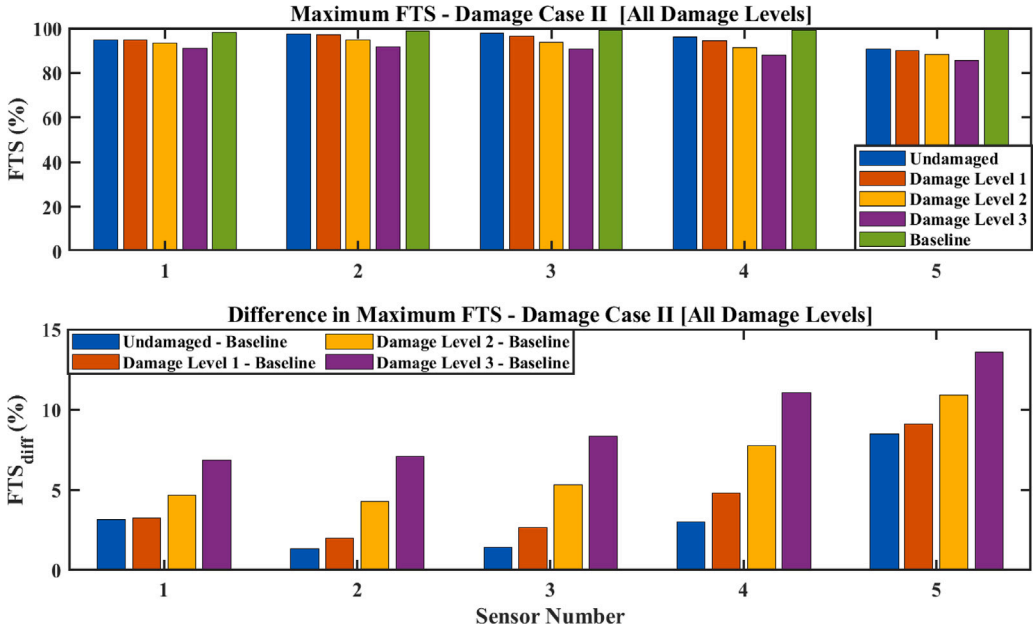

Fig. 9. Maximum FTS values and the difference between these values and the baseline, FTS_{diff}, for different damage levels at the location of each sensor for the 5-story RC building for damage case II under the ground motion RSN21.

a variety of sensors, including accelerometers on the foundation and on each floor to record accelerations. Figs. 14 and 15 show the three-dimensional view and plan views of each floor of the test concrete wall building, respectively.

This test building was tested for different near-fault and far-field earthquakes. These tests were conducted under increasing intensities of the applied ground motions from 25% to 180% and acceleration measurements were obtained at each floor on the slabs and walls. From the available datasets, the ground motion intensities of 25%, 50%, and 100% and different design configurations of the test building denoted by **D1a**, **D1b**, **D1c**, and **D2** were used to define undamaged and different damaged states of the building in this study. The considered datasets and a brief description of corresponding undamaged and defined damaged states at each level are as follows,

- Undamaged: dataset D1a-25%; at the intensity of 25% of the applied ground motion tests, only very few small cracks with maximum widths of 0.2 mm were observed on the building at beam interfaces and under some of the link slabs perpendicular to walls.
- Damage level 1: dataset D1a-50%; at the seismic intensity of 50%, more cracks on the top of beams and perpendicular to the beam-wall interfaces, continuous cracks, and cracks of widths exceeding 0.2 mm were observed.
- Damage level 2: dataset D1b-100%; at the 100% seismic intensity, new cracks were developed around corners and beam joints, new cracks were found along the beam interfaces, cracks perpendicular to a wall further extended into the floor, and crack widths of more than 0.3 mm were observed.
- Damage level 3: dataset D1c-100%
- Damage level 4: dataset D2%–100%; at the applied 100% seismic intensity in this dataset, several new cracks parallel to beam-wall interfaces and perpendicular across link slabs were found, and some minor spalling of a wall on the top of the first floor was observed. Widest cracks concentrated at ends of a wall at the top of the first floor, new diagonal cracks extended into the floor slab from wall-floor connections at the top of the second floor, and widening of cracks at beam interfaces, slotted joints, and wall ends up to 0.6 mm of the crack widths were found.

Acceleration data from the following 10 accelerometer sensors were used for analyses,

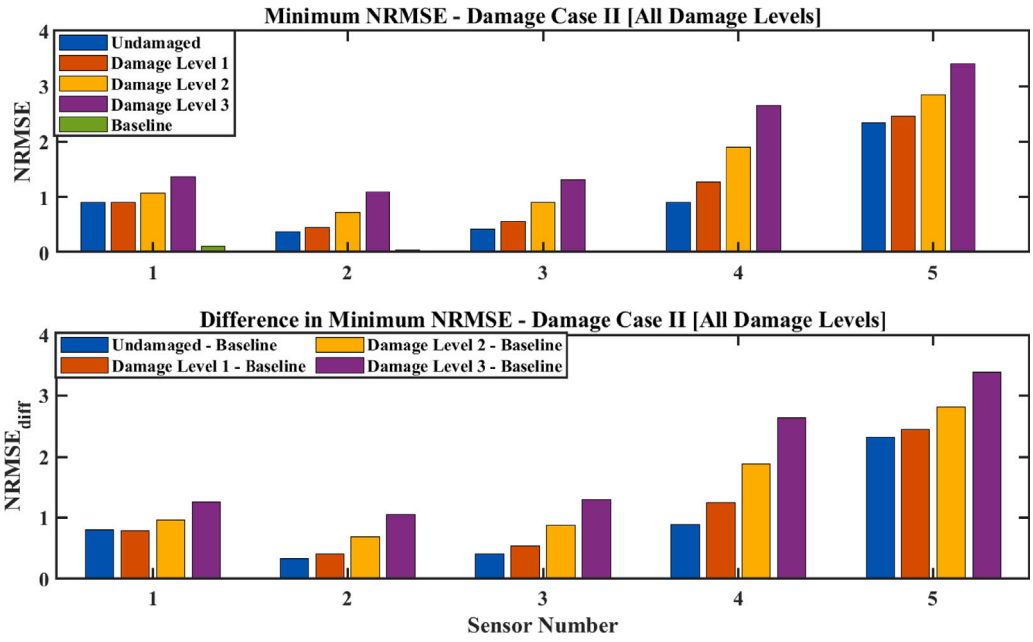

Fig. 10. Minimum NRMSE values and the difference between these values and the baseline, $NRMSE_{diff}$, for different damage levels at the location of each sensor for the 5-story RC building for damage case II under the ground motion RNS21.

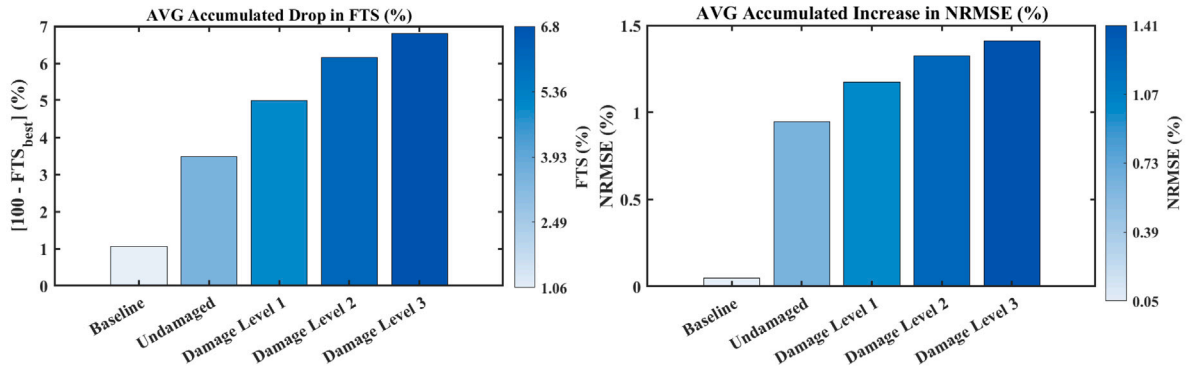

(a) Averaged accumulated drop in FTS (b) Averaged accumulated increase in NRMSE

Fig. 11. Average accumulated drop in FTS and increase in NRMSE for damage case III for the 5–story RC building under the ground motion RSN21; AVG: Average.

1. A-L1-Floor-A1-EW
2. A-L1-Floor-A2-EW
3. A-L1-Floor-B1-EW
4. A-L1-Floor-B2-EW
5. A-L1-Wall-B1-EW
6. A-L2-Floor-A1-EW
7. A-L2-Floor-A2-EW
8. A-L2-Floor-B1-EW
9. A-L2-Floor-B2-EW
10. A-L2-Wall-B1-EW

In the above notations, A stands for the accelerometer sensor, EW denotes the East-West direction for measurements, L1 and L2, represent the first and second floors of the building, respectively, while A1, A2, B1, and B2, represent the axes of the building plan. The shake table accelerations measured in the longitudinal direction were used as the input ground excitations. Further details on the test structure, used sensors, description of the tests, above datasets, and applied ground motions can be found in [89] and the above-mentioned open-source archive of the datasets.

3.5.1. PGA level classification

The test building was tested under ground motions at different levels of PGA's. As the PGA intensities of the applied ground motions gradually increased from the beginning up to the end through different tests, the building experienced different damage states, which would force the structures' responses into nonlinear regions. Therefore, to keep the accuracy of analyses in the proposed approach for handling these different regions, the building's responses were considered as signals with separate regions in terms of PGA values, and two main PGA levels were defined when analyzing the acceleration data as follows,

- **Medium-Level PGA**: The acceleration data with values **below 0.1** g were considered as Medium-Level PGA values. Both the initial range (acceleration values from 0.01 g to 0.1 g) and the final range (acceleration values from 0.1 g back to 0.01 g) were merged as one dataset for the analysis.
- **High-Level PGA**: The acceleration data with values **above 0.1** g were categorized as High-Level PGA values. Acceleration records from the first instance above 0.1 g to the last instance above 0.1 g were used for the analysis.

3.5.2. Damage assessment of the full-scale building by the proposed technique

The acceleration data from accelerometers as listed above from the selected datasets for undamaged and defined damaged states were

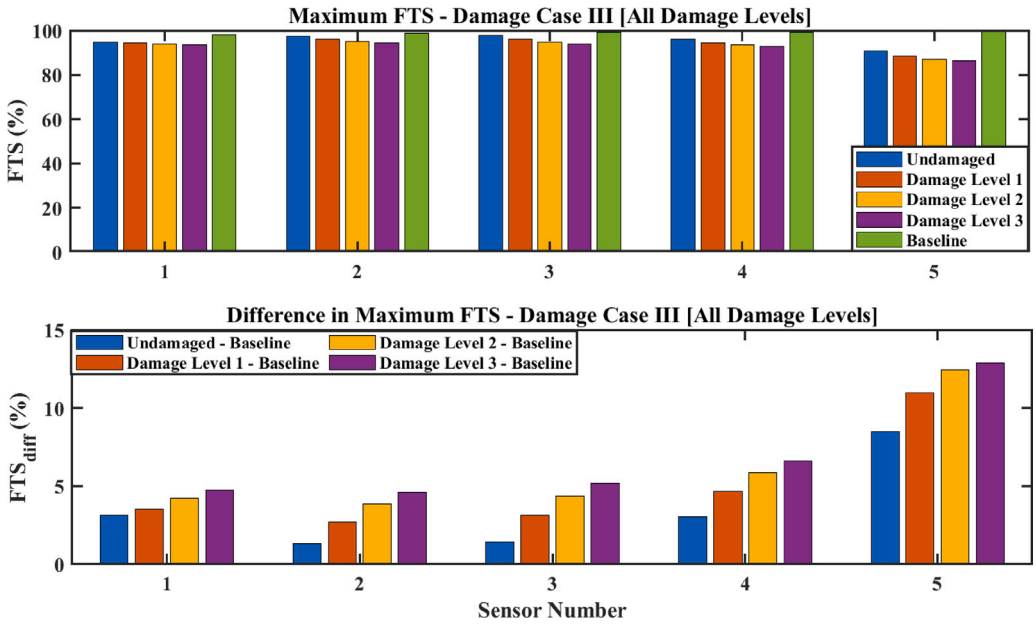

Fig. 12. Maximum FTS values and the difference between these values and the baseline, FTS_{diff}, for different damage levels at the location of each sensor for the 5-story RC building for damage case III under the ground motion RSN21.

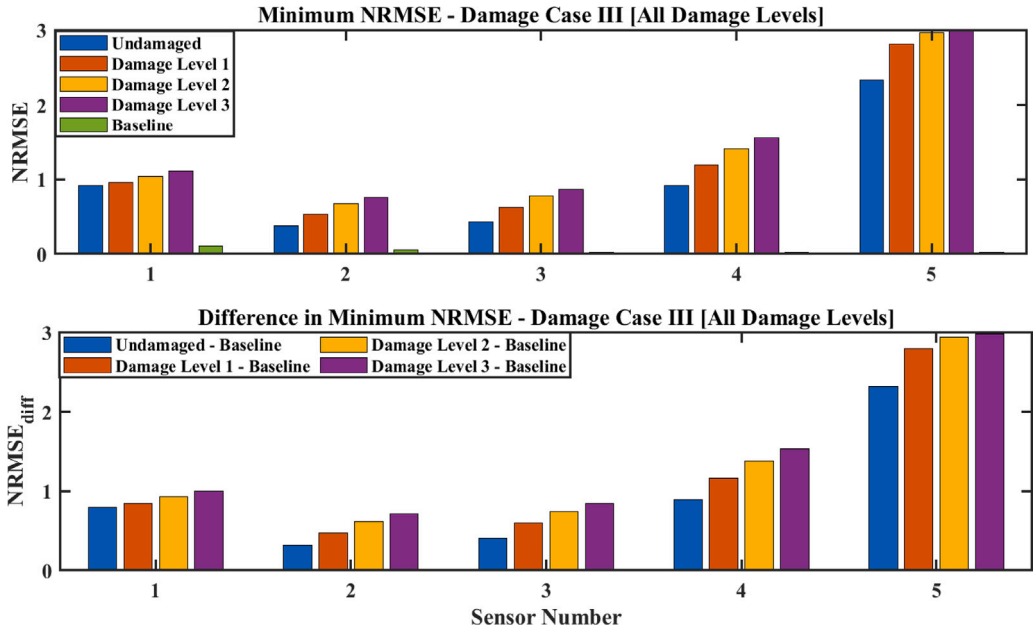

Fig. 13. Minimum NRMSE values and the difference between these values and the baseline, $NRMSE_{diff}$, for different damage levels at the location of each sensor for the 5-story RC building for damage case III under the ground motion RNS21.

utilized in the proposed SHM technique. The corresponding FTS and NRMSE values have been calculated and diagrammed for the 10 accelerometer sensors as shown in Figs. 16 to 21 for both Medium-Level and High-Level PGA classifications described above.

As seen in these figures, the bars corresponding to the Undamaged case for average accumulated drop in FTS, average accumulated increase in NRMSE, and (Undamaged - Baseline) in FTS_{diff} and $NRMSE_{diff}$ are always equal to zero. This is because only a single data file was available for the undamaged condition in the applied datasets, resulting in no variations in results other than damage levels. A clearer indication of damage progression from Damage Level 1 to 4 has been represented by the method through average accumulated drop in FTS in Fig. 17(a) under High-Level PGA, while Fig. 16(b), which represents evaluations under Medium-Level PGA shows a clear ascending trend of NRMSE with damage progression. In Fig. 20 for maximum FTS values calculated under High-Level PGA, a clear indication of damage progression from Damage Level 1 to 4 is obvious for all 10 sensors, while such an indication under Medium-Level PGA values can be found for accelerometer sensors 1 to 4, and fluctuations for the rest of the sensors according to Fig. 18. Also, examining Figs. 19 and 21 demonstrate a consistent increasing trend of NRMSE for most of the sensors by progressing the damage state under the Medium-Level PGA in the former figure, while in the latter figure, such a clear indication can be seen from Damage Level 2 to 4 for most of the sensors. Even though some fluctuations across different sensors were found when evaluating the best FTS and minim NRMSE, examining these figures further confirms the performance of the proposed technique as demonstrated for the numerical experiment, including a decrease

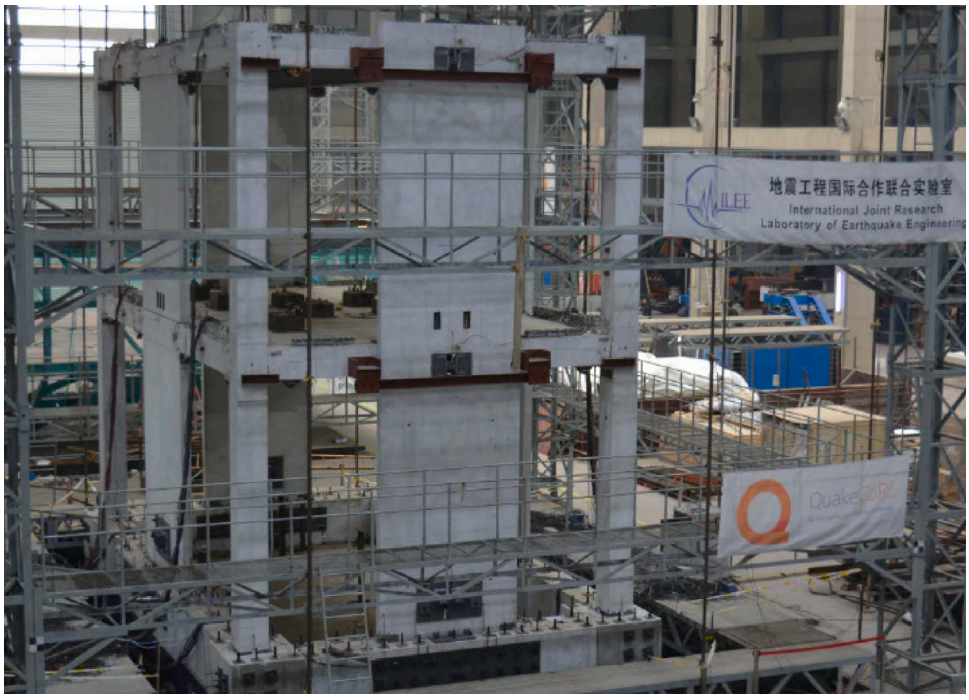

Fig. 14. Two-story concrete wall test building; adopted from Lu et al. 2021 [89].

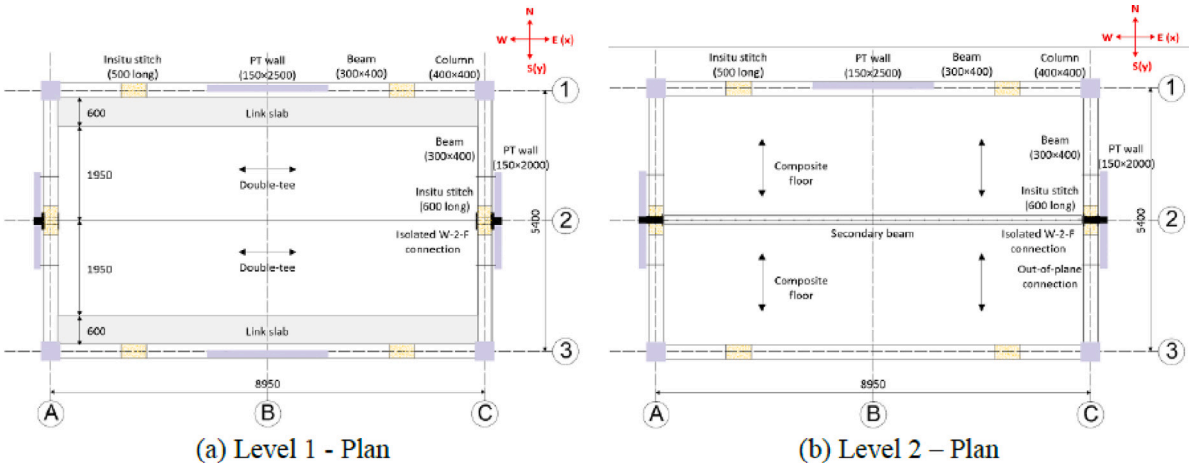

Fig. 15. Plan view of each floor for the two-story concrete wall test building; adopted from Lu et al. 2021 [89].

in FTS and an increase in NRSME values with progression of damage from levels 1 to 4, similar performance levels for all sensors at different damage levels, and close proximity of FTS_{max} and $NRMSE_{min}$ values for all sensors at different damage levels.

4. Conclusions

In this paper, a novel SHM technique for damage detection and progression has been put forward. The proposed methodology uses an ARX model as an adaptive TS model to detect damage and its progression in a building structure. Using the proposed approach, the historical data that have been recorded at instrumented buildings can be utilized to develop baseline models. New recordings can be used for real-time damage detection or updating the baseline models. The proposed method has been meticulously developed to facilitate practical condition assessments of buildings subjected to ground motion excitations. Its design inherently supports applications in scenarios where sensor availability is extremely limited. In fact, the methodology is fully applicable even when the building instrumentation is restricted to only two sensors – one deployed at the ground level and the other affixed to the structure – and can be used with similar TS techniques that work based on only input/output data.

To demonstrate the performance of the proposed technique, a 5-story RC building was modeled using SAP2000 software platform. The building was instrumented using five sensors in one gridline and different damage cases and levels were defined. The model was examined under 20 ground motions for developing the ARX models for each sensor based on the input/output data. The effect of frequency shifts due to the defined damage levels was examined using the modal analysis which showed intangible changes that cannot be detected using frequency shift-based SHM approaches. FTS and NRMSE values were calculated and comparative studies were conducted for the introduced damage cases at different damage levels. Results of the analytical simulations showed that the method is robust to sensor proximity to the damage location, and has high sensitivity to damage progression by detecting small changes in the FTS and NRMSE values by increasing

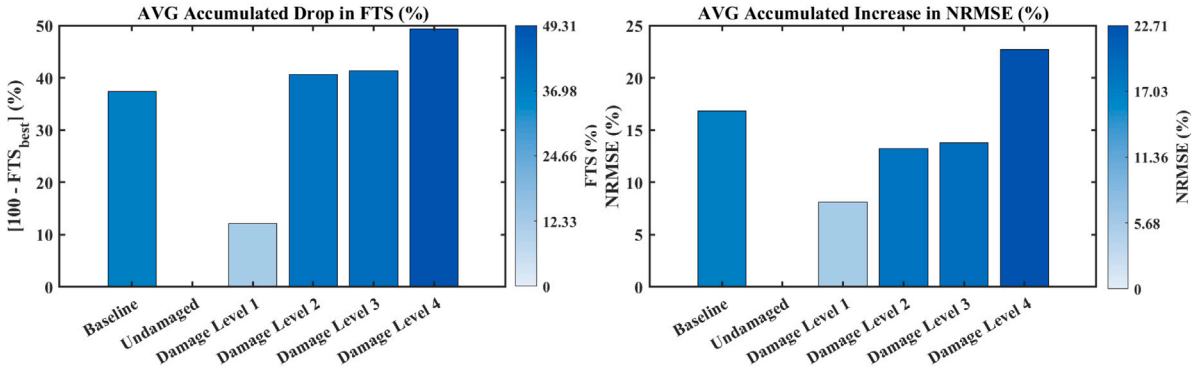

(a) Averaged accumulated drop in FTS (b) Averaged accumulated increase in NRMSE

Fig. 16. Average accumulated drop in FTS and increase in NRMSE for different damage levels for the test two-story concrete wall building under **Medium-Level PGA**; AVG: Average.

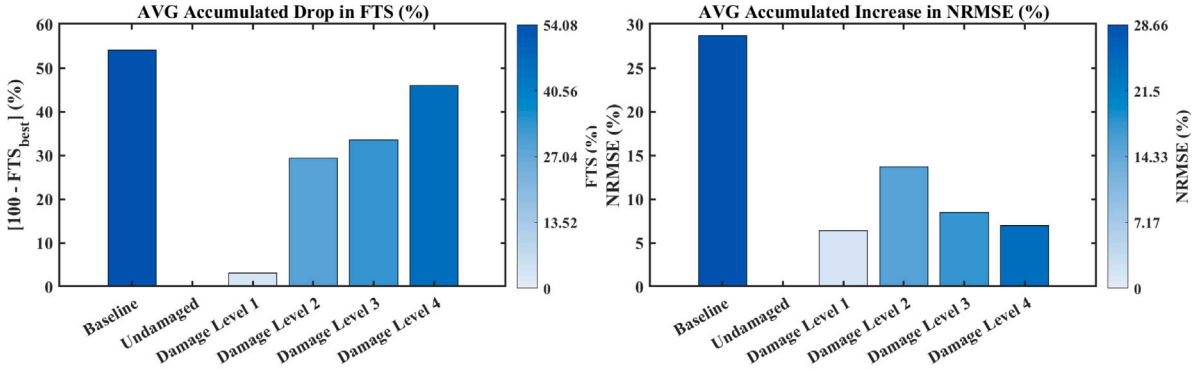

(a) Averaged accumulated drop in FTS (b) Averaged accumulated increase in NRMSE

Fig. 17. Average accumulated drop in FTS and increase in NRMSE for different damage levels for the test two-story concrete wall building under **High-Level PGA**; AVG: Average.

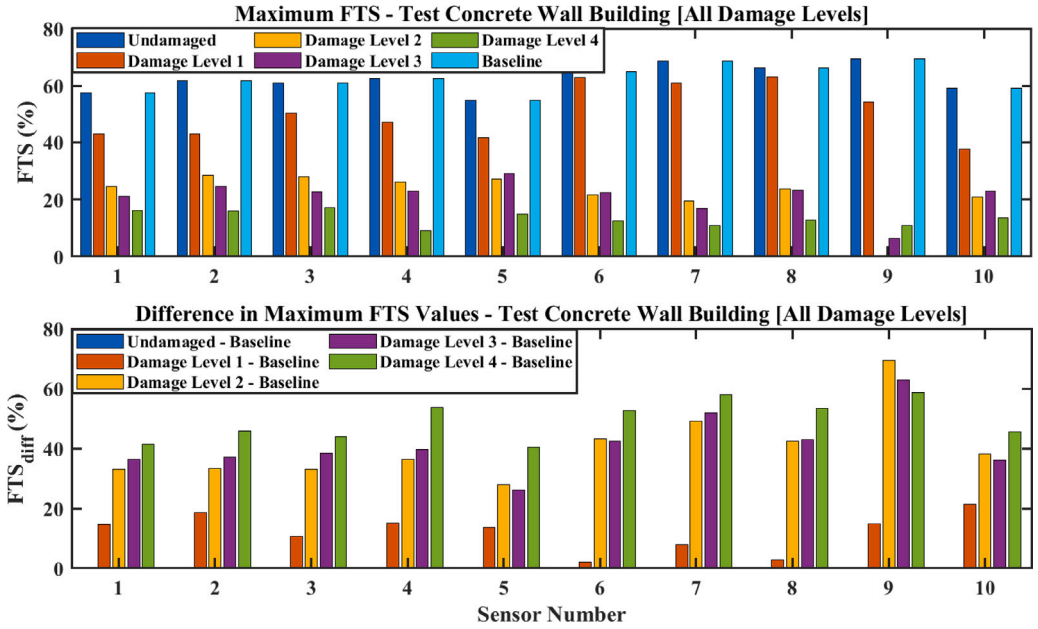

Fig. 18. Maximum FTS values and the difference between these values and the baseline, FTS_{diff}, for different damage levels at the location of each sensor for the 10 selected sensors on the test two-story concrete wall building under **Medium-Level PGA**.

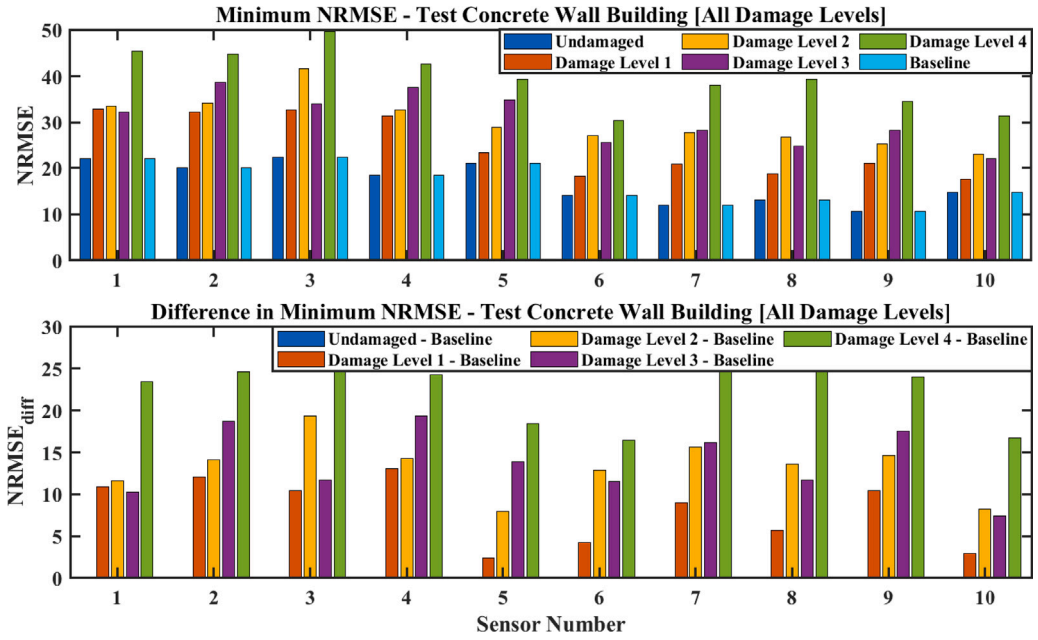

Fig. 19. Minimum NRMSE values and the difference between these values and the baseline, $NRMSE_{diff}$, for different damage levels at the location of each sensor for the 10 selected sensors on the test two-story concrete wall building under **Medium-Level PGA**.

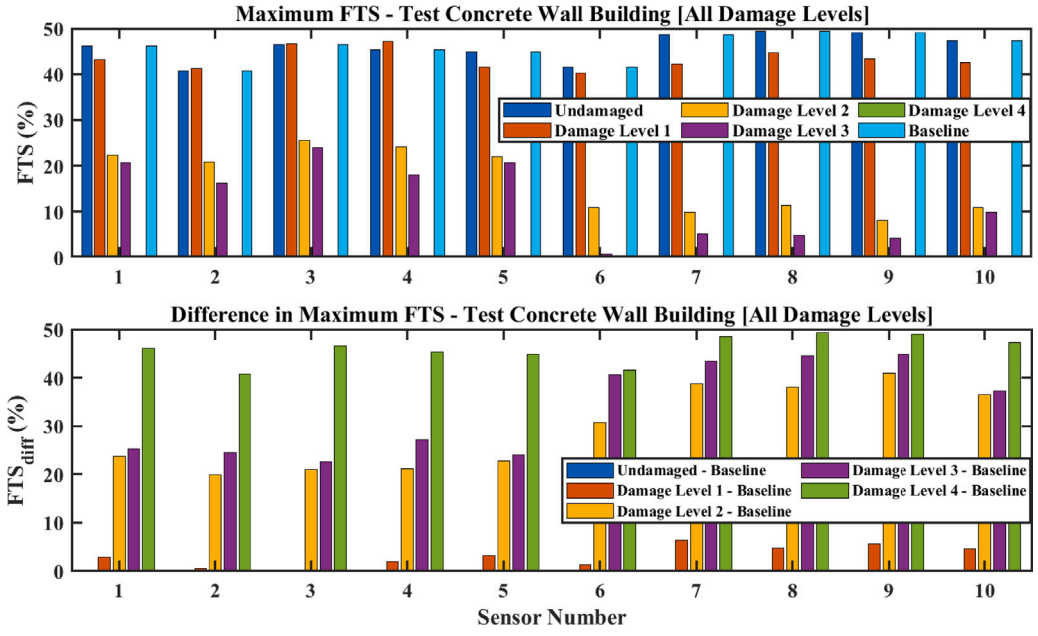

Fig. 20. Maximum FTS values and the difference between these values and the baseline, FTS_{diff}, for different damage levels at the location of each sensor for the 10 selected sensors on the test two-story concrete wall building under **High-Level PGA**.

the damage level in the structure. Moreover, the application of two ground motions with different characteristics proved the robustness of the technique in damage detection under ground motions with different characteristics. Furthermore, the sensory data from open-source datasets available for experimental tests of a full-scale two-story post-tensioned concrete wall building instrumented with accelerometer sensors for damage assessments were employed to further examine the performance of the proposed methodology. Results of investigations in this section additionally demonstrated the practicality and efficacy of the technique when applied to a full-scale building by confirming the results of analyses similar to those demonstrated for the numerical simulation.

Numerical investigations and further confirmation of the results against experimental tests of a full-scale concrete wall building proved the viability of the proposed approach for damage detection and progression with a minimum number of sensors. The rigorous numerical

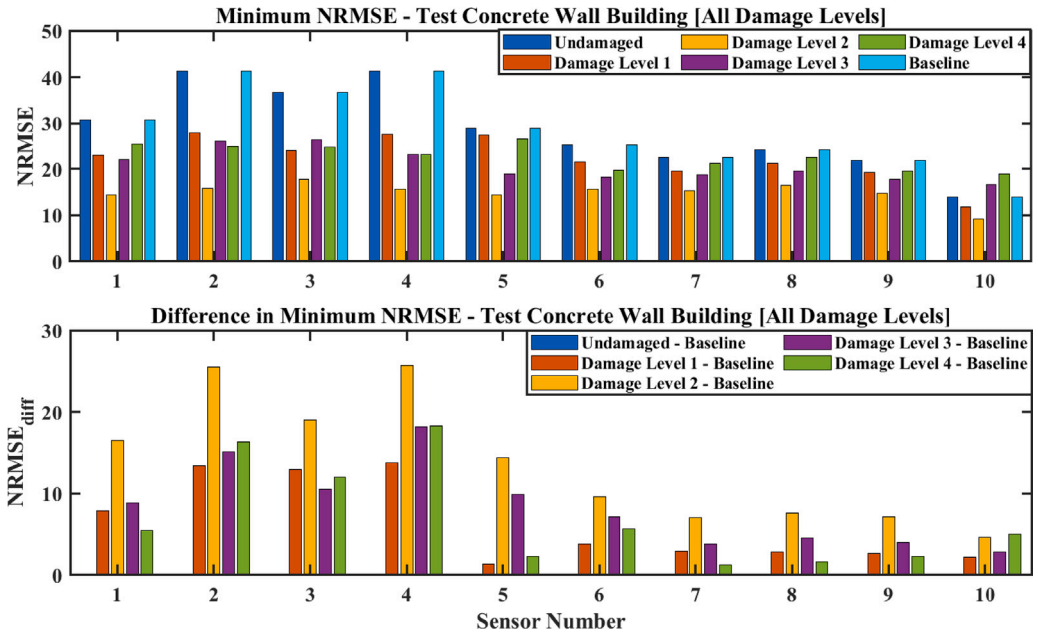

Fig. 21. Minimum NRMSE values and the difference between these values and the baseline, $NRMSE_{diff}$, for different damage levels at the location of each sensor for the 10 selected sensors on the test two-story concrete wall building under **High-Level PGA**.

analyses and additional validation through experimental data conducted in this research offer robust evidence of the method's performance and the efficiency of the approach in real-world structural health monitoring applications.

CRediT authorship contribution statement

Sherif Beskhyroun: Writing – review & editing, Writing – original draft, Visualization, Validation, Supervision, Resources, Project administration, Methodology, Investigation, Formal analysis, Data curation, Conceptualization. **Seyed Ehsan Aghakouchaki Hosseini:** Writing – review & editing, Writing – original draft, Visualization, Validation, Investigation.

Declaration of competing interest

The authors declare that they have no known competing financial interests or personal relationships that could have appeared to influence the work reported in this paper.

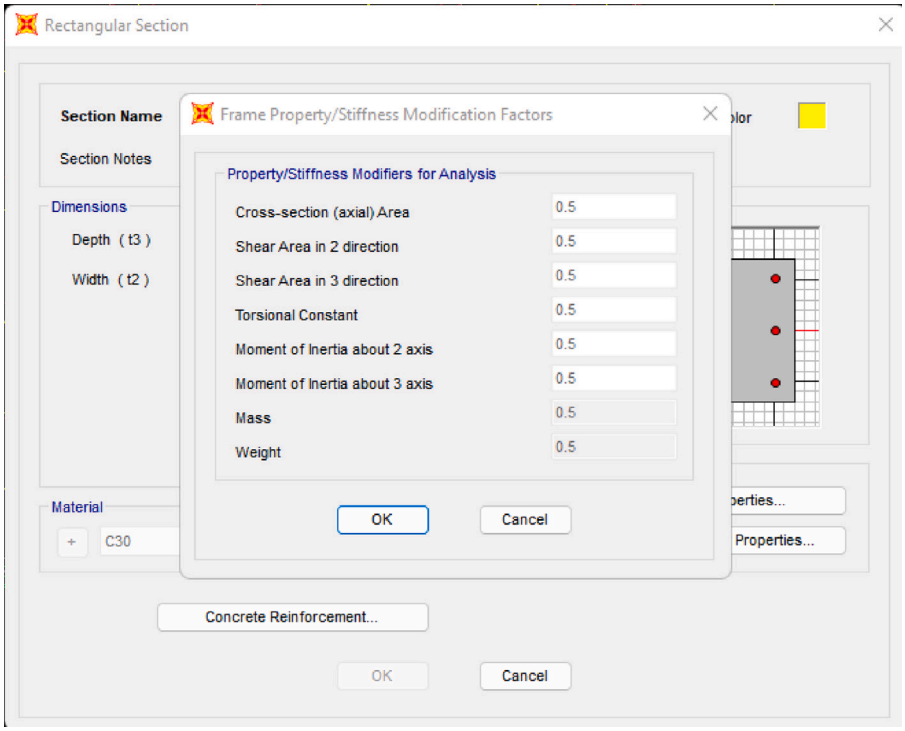

Fig. A.22. Section properties reduction in SAP2000 to define damage.

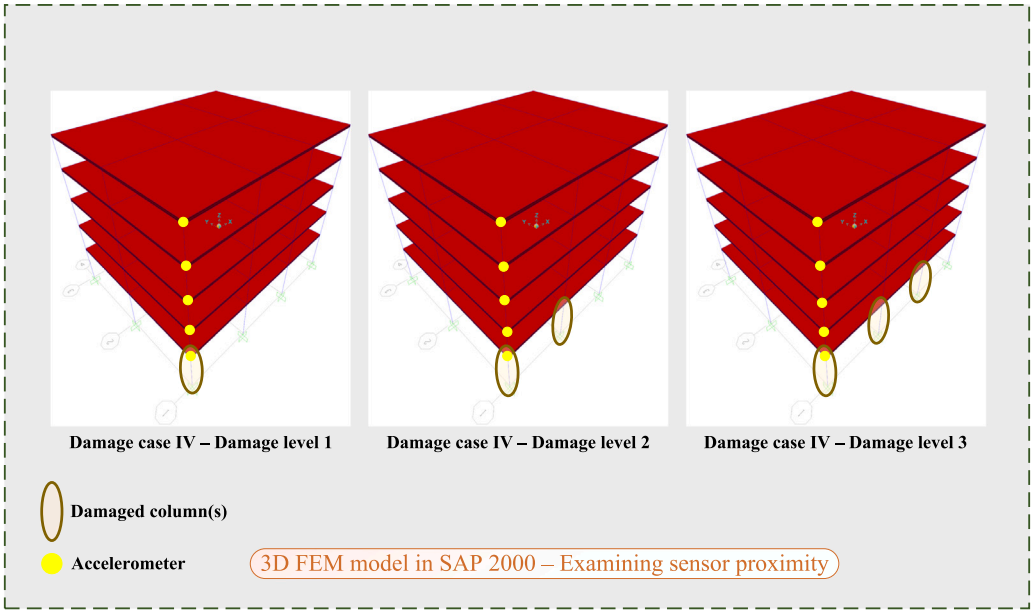

(a) Damage case IV at three damage levels

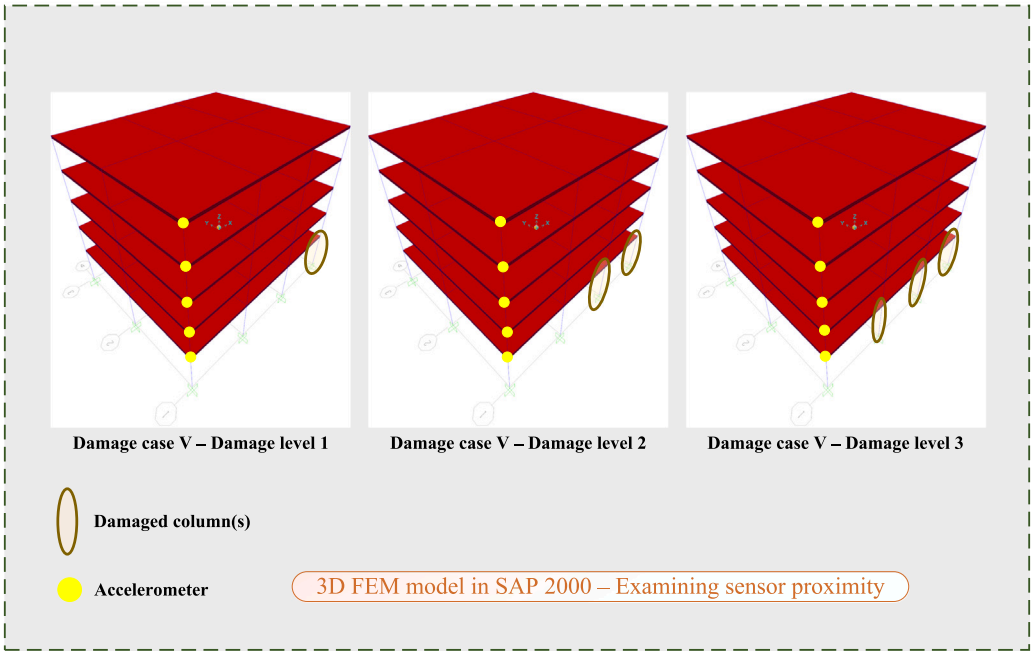

(b) Damage case V at three damage levels

Fig. A.23. 3D model of the 5-story RC building under ground motion RSN21 modeled in SAP2000 instrumented with sensors to examine sensor proximity on the performance of the proposed SHM technique: (a) different damage levels for damage case IV, (b) different damage levels for damage case V.

Appendix. Examinations for sensor proximity, high-level damage, ground motion characteristics, and damage in other stories

A damage scenario by reducing the cross-sectional properties of the columns in only one xfloor on specific gridlines of the structure by 50% as shown in Fig. A.22 was introduced and three damage cases were examined, each at three damage levels.

To assess the performance of the proposed approach for high-level damage, while accelerometers are at gridline 1-A, a damage case (IV) at different damage levels under the ground motion RSN21 was introduced as follows,

- **Damage case IV - damage level 1:** 50% reduction in section properties for the column at gridline 1-A at the ground level only.
- **Damage case IV - damage level 2:** 50% reduction in section properties for columns at gridlines 1-A and 1-B at the ground level only.

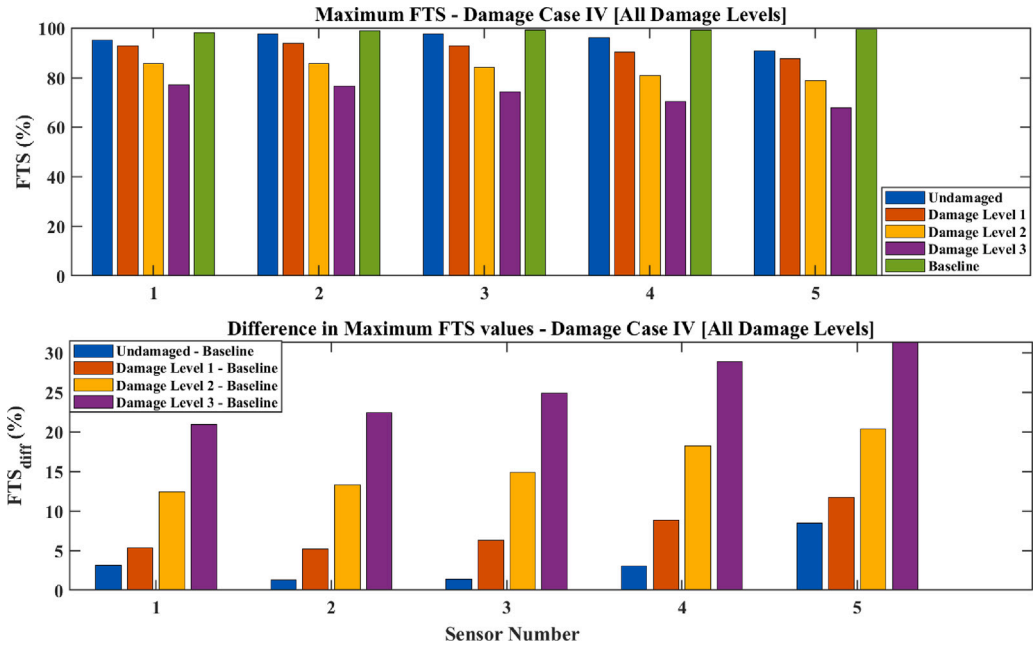

Fig. A.24. Maximum FTS values and the difference between these values and the baseline, FTS_{diff}, for different damage levels at the location of each sensor for the 5-story RC building for damage case IV under ground motion RSN21.

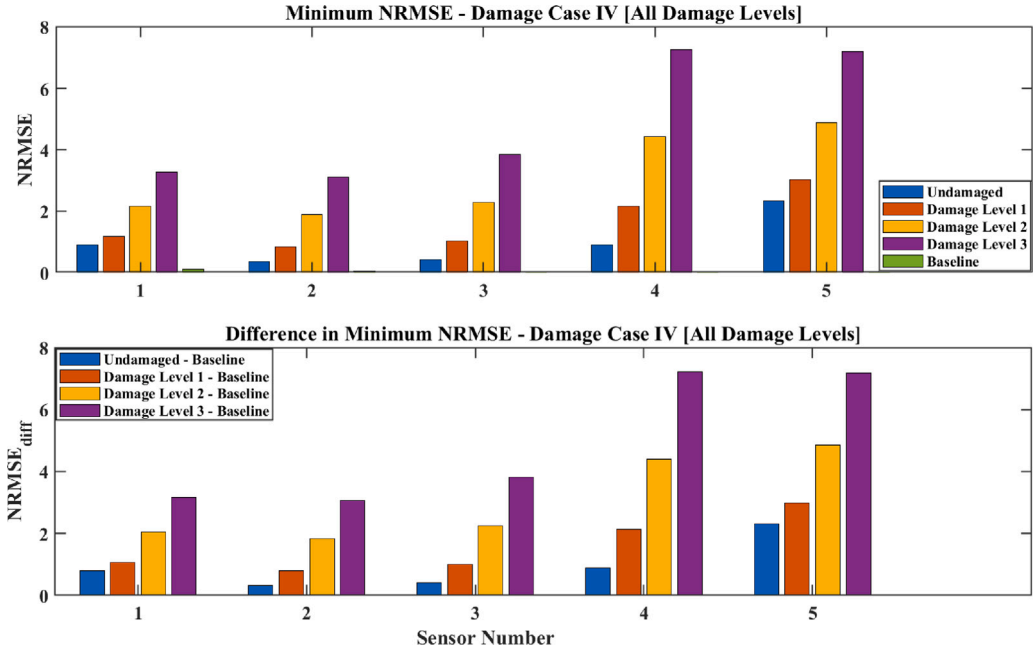

Fig. A.25. Minimum NRMSE values and the difference between these values and the baseline, $NRMSE_{diff}$, for different damage levels at the location of each sensor for the 5-story RC building for damage case IV under ground motion RSN21.

- **Damage case IV - damage level 3:** 50% reduction in section properties for columns at gridlines 1-A, 1-B, and 1-C at the ground level only.

By keeping the accelerometer sensors at the same locations (gridline 1-A, floors 1–5), two other damage scenarios are examined.

To examine the impact of the sensor proximity to damaged locations, a new damage case (V) under the same RSN21 ground motion at different damage levels was introduced as follows,

- **Damage case V - damage level 1:** 50% reduction in section properties for the column at gridline 1-D at the ground level only.
- **Damage case V - damage level 2:** 50% reduction in section properties for columns at gridlines 1-D and 1-C at the ground level only.
- **Damage case V - damage level 3:** 50% reduction in section properties for columns at gridlines 1-D, 1-C, and 1-B at the ground level only.

These damage cases and levels have been illustrated in Fig. A.23 (a,b).

To assess the influence of the ground motion characteristics on damage detection accuracy, a new damage case (VI) under the ground motion RSN25 at different damage levels was introduced as follows,

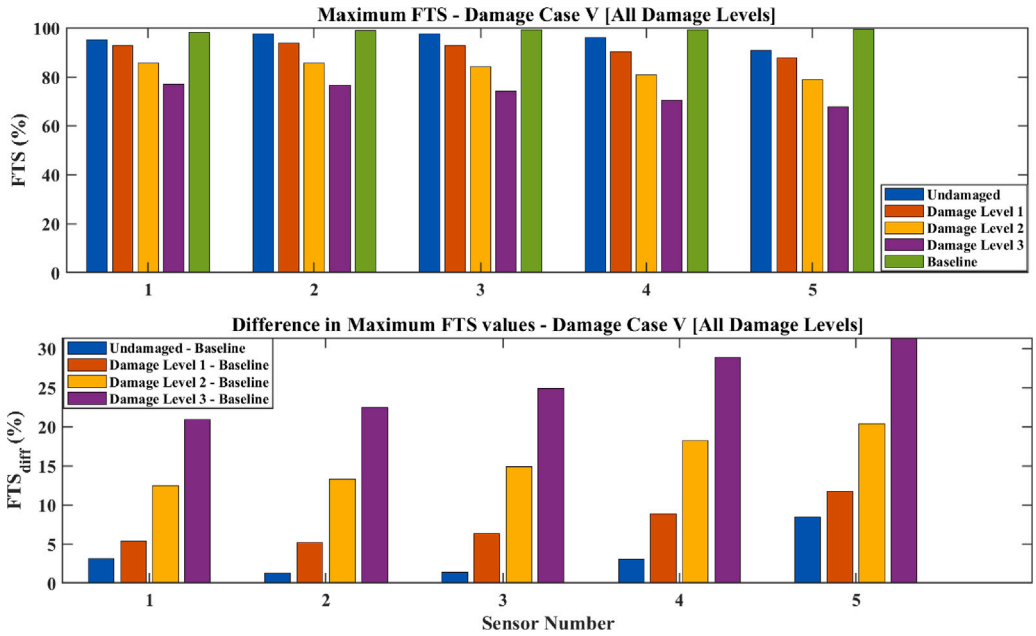

Fig. A.26. Maximum FTS values and the difference between these values and the baseline, FTS_{diff}, for different damage levels at the location of each sensor for the 5-story RC building for damage case V under ground motion RSN21.

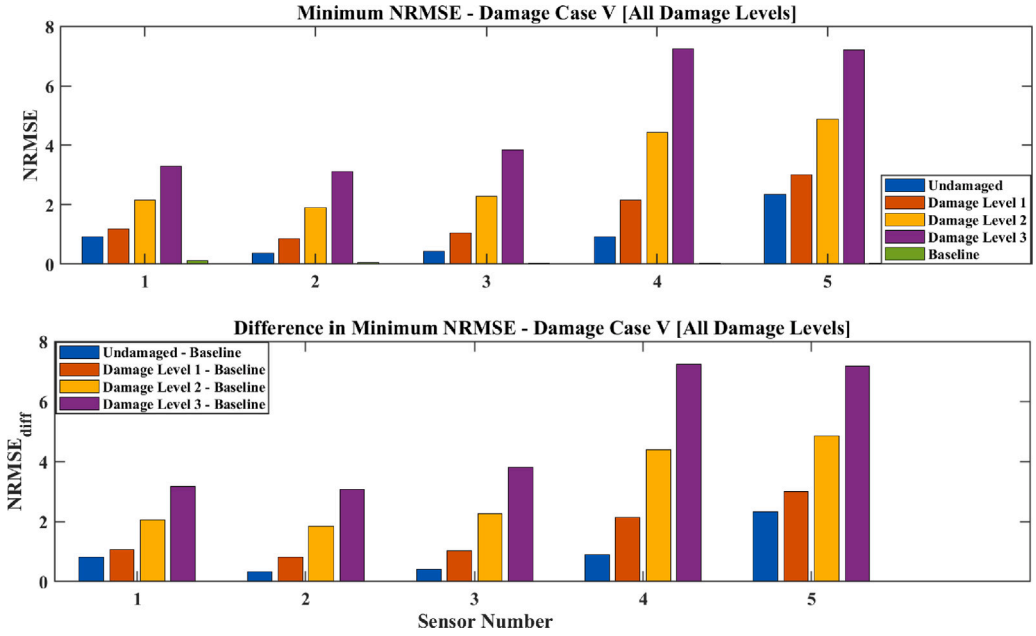

Fig. A.27. Minimum NRMSE values and the difference between these values and the baseline, $NRMSE_{diff}$, for different damage levels at the location of each sensor for the 5-story RC building for damage case V under ground motion RSN21.

- **Damage case VI - damage level 1:** 50% reduction in section properties for the column at gridline 1-A at the ground level only.
- **Damage case VI - damage level 2:** 50% reduction in section properties for columns at gridlines 1-A and 1-B at the ground level only.
- **Damage case VI - damage level 3:** 50% reduction in section properties for columns at gridlines 1-A, 1-B, and 1-C at the ground level only.

It is noteworty that this damage case is in fact similar to damage case IV in terms of damage definition but only investigated under a different ground motion. To further evaluate the technique for damage location, another damage case (VII) was introduced at the 3rd floor of the structure at different damage levels under ground motion RSN21, as follows,

- **Damage case VII - damage level 1:** 50% reduction in section properties for the column at gridline 1-A on the **3rd floor** of the building.
- **Damage case VII - damage level 2:** 50% reduction in section properties for columns at gridlines 1-A and 1-B on the **3rd floor** of the building.
- **Damage case VII - damage level 3:** 50% reduction in section properties for columns at gridlines 1-A, 1-B, and 1-C on the **3rd floor** of the building.

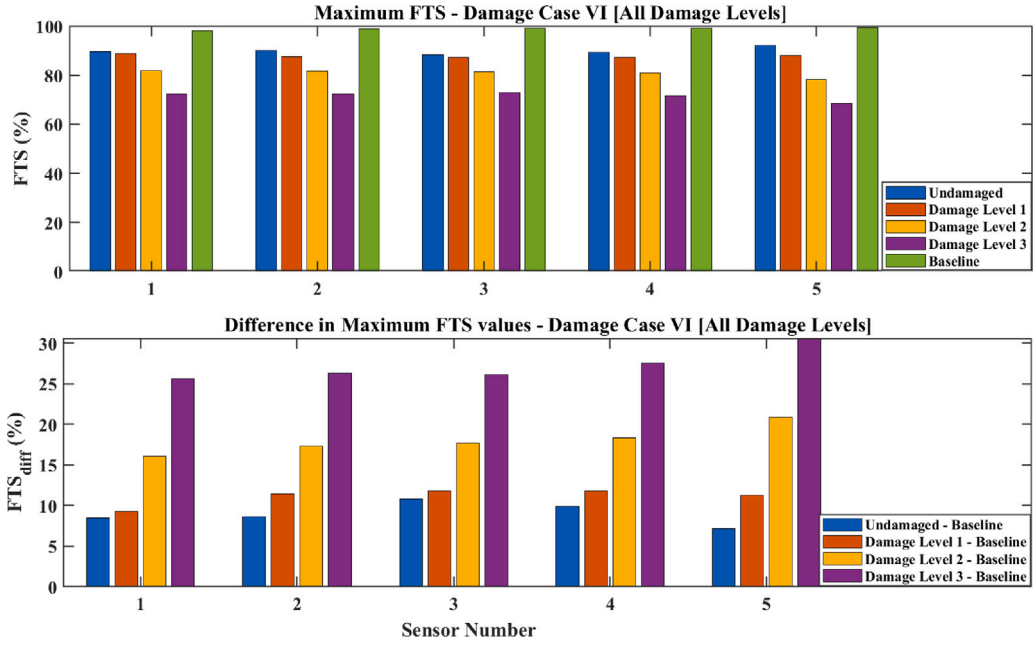

Fig. A.28. Maximum FTS values and the difference between these values and the baseline, FTS_{diff}, for different damage levels at the location of each sensor for the 5-story RC building for damage case VI under ground motion RSN25.

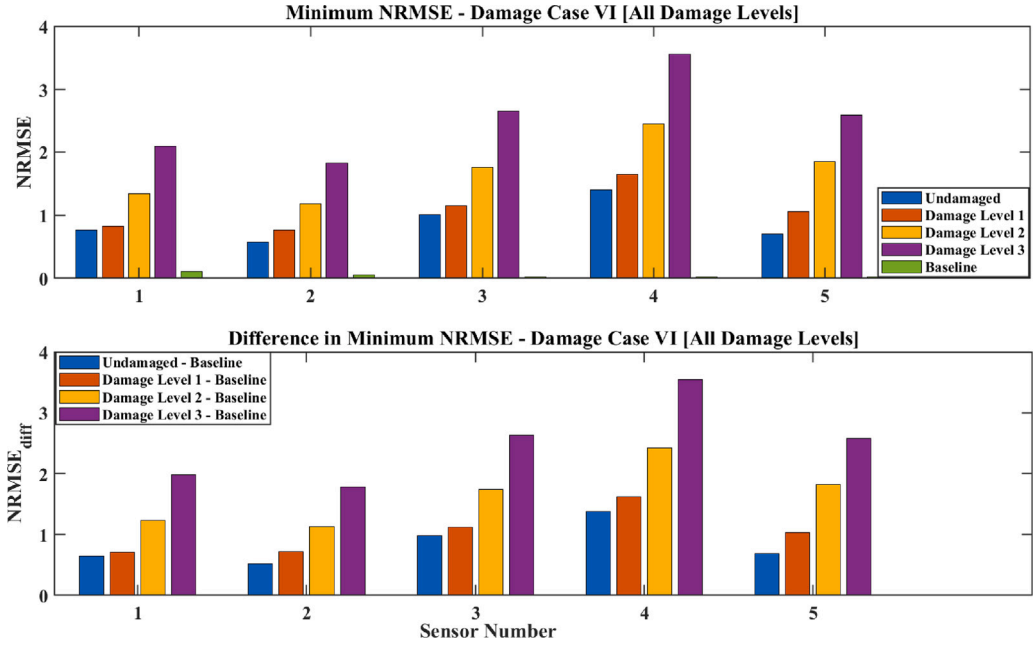

Fig. A.29. Minimum NRMSE values and the difference between these values and the baseline, $NRMSE_{diff}$, for different damage levels at the location of each sensor for the 5-story RC building for damage case VI under ground motion RSN25.

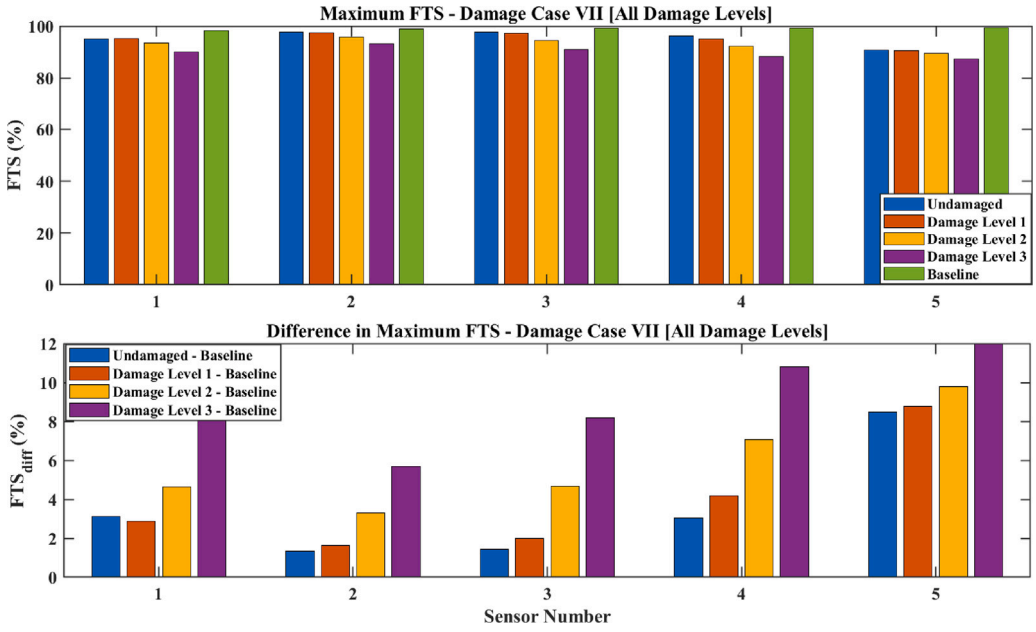

Fig. A.30. Maximum FTS values and the difference between these values and the baseline, FTS_{diff}, for different damage levels at the location of each sensor for the 5-story RC building for damage case VII (**3rd floor**) under ground motion RSN21.

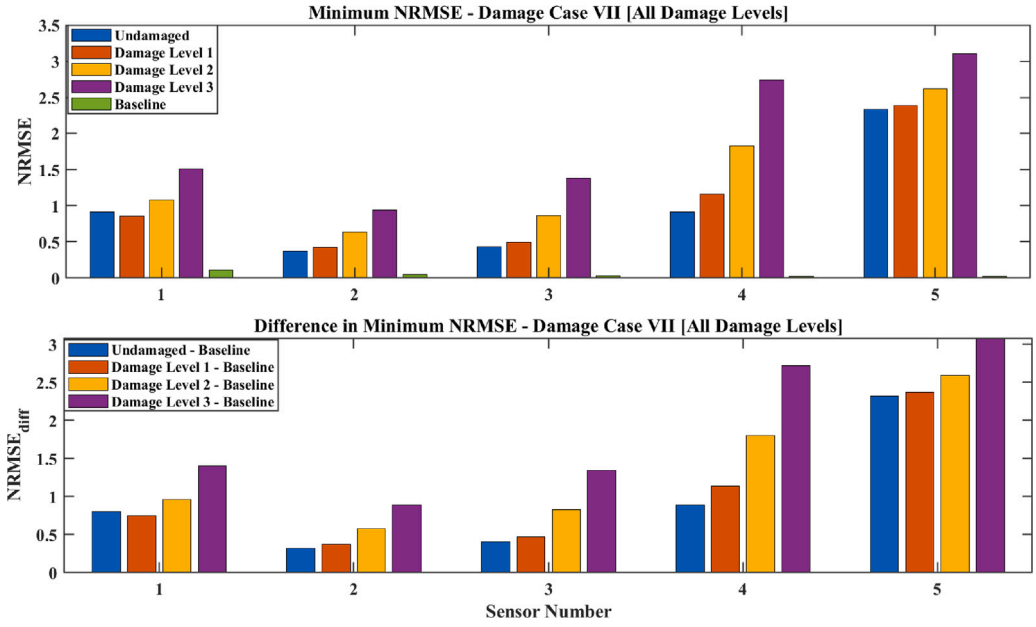

Fig. A.31. Minimum NRMSE values and the difference between these values and the baseline, $NRMSE_{diff}$, for different damage levels at the location of each sensor for the 5-story RC building for damage case VII (**3rd floor**) under ground motion RSN25.

Data availability

Data will be made available on request.

References

[1] Gharehbaghi VR, Nguyen A, Farsangi EN, Yang TY. Supervised damage and deterioration detection in building structures using an enhanced autoregressive time-series approach. J Build Eng 2020;30:101292.

[2] Deng Y, Zhao Y, Ju H, Yi T-H, Li A. Abnormal data detection for structural health monitoring: State-of-the-art review. Dev Built Environ 2024;100337.

[3] Navabian N, Beskhyroun S, Matulich J. Development of wireless smart sensor network for vibration-based structural health monitoring of civil structures. Struct Infrastruct Eng 2022;18(3):345–61.

[4] Hosseini SEA, Beskhyroun S. Fluid storage tanks: A review on dynamic behaviour modelling, seismic energy-dissipating devices, structural control, and structural health monitoring techniques. In: Structures. vol. 49, Elsevier; 2023, p. 537–56.

[5] Loutas TH, Panopoulou A, Roulias D, Kostopoulos V. Intelligent health monitoring of aerospace composite structures based on dynamic strain measurements. Expert Syst Appl 2012;39(9):8412–22.

[6] Camarena-Martinez D, Osornio-Rios R, Romero-Troncoso R, Garcia-Perez A. Fused empirical mode decomposition and MUSIC algorithms for detecting multiple combined faults in induction motors. J Appl Res Technol 2015;13(1):160–7.

[7] Wang M, Incecik A, Tian Z, Zhang M, Kujala P, Gupta M, Krolczyk G, Li Z. Structural health monitoring on offshore jacket platforms using a novel ensemble deep learning model. Ocean Eng 2024;301:117510.

[8] Komarizadehasl S, Jiménez MAG, Casas JMP, Lozano-Galant JA, Turmo J. Eigenfrequency analysis using fiber optic sensors and low-cost accelerometers for structural damage detection. Eng Struct 2024;318:118684.

[9] Park HS, Kim JM, Choi SW, Kim Y. A wireless laser displacement sensor node for structural health monitoring. Sens 2013;13(10):13204–16.

[10] Lee E-T, Eun H-C. Damage detection of beam structure using response data measured by strain gages. J Vibroengineering 2014;16(1):147–55.

[11] Ferreira J, Branco F. Measurement of vertical deformations in bridges using an innovative elastic cell system. Exp Tech 2015;39:13–20.

[12] Abdullah A, Rice JA, Hamilton H, Consolazio GR. Experimental and numerical evaluation of unbonded posttensioning tendons subjected to wire breaks. J Bridg Eng 2016;21(10):04016066.

[13] Enckell M, Egede Andersen J, Glisic B, Silfwerbrand J. New and emerging technologies in structural health monitoring. 2013.

[14] Bonopera M. Fiber-bragg-grating-based displacement sensors: Review of recent advances. Mater 2022;15(16):5561.

[15] Di Trapani F, Oddo MC, Sberna AP, La Mendola L. Structural health monitoring of masonry structures using stress sensors: Experimental induced damage tests and proposed approach for real-time monitoring. Constr Build Mater 2024;449:138077.

[16] Chen C-C, Wu W-H, Tseng H-Z, Chen C-H, Lai G. Application of digital photogrammetry techniques in identifying the mode shape ratios of stay cables with multiple camcorders. Meas 2015;75:134–46.

[17] Oh BK, Hwang JW, Kim Y, Cho T, Park HS. Vision-based system identification technique for building structures using a motion capture system. J Sound Vib 2015;356:72–85.

[18] Yang Y, Dorn C, Mancini T, Talken Z, Kenyon G, Farrar C, Mascareñas D. Blind identification of full-field vibration modes from video measurements with phase-based video motion magnification. Mech Syst Signal Process 2017;85:567–90.

[19] Moreno-Gomez A, Perez-Ramirez CA, Dominguez-Gonzalez A, Valtierra-Rodriguez M, Chavez-Alegria O, Amezquita-Sanchez JP. Sensors used in structural health monitoring. Arch Comput Methods Eng 2018;25:901–18.

[20] Zhang H, Reuland Y, Shan J, Chatzi E. Post-earthquake structural damage assessment and damage state evaluation for RC structures with experimental validation. Eng Struct 2024;304:117591.

[21] Limongelli MP, Çelebi M. Seismic structural health monitoring: from theory to successful applications. Springer; 2019.

[22] Meruane V, Heylen W. An hybrid real genetic algorithm to detect structural damage using modal properties. Mech Syst Signal Process 2011;25(5):1559–73.

[23] Chesné S, Deraemaeker A. Damage localization using transmissibility functions: A critical review. Mech Syst Signal Process 2013;38(2):569–84.

[24] Sen N, Gupta VK. On estimation of seismic damage from ductility and hysteretic energy demands in equivalent oscillators using linear response. Eng Struct 2018;172:663–86.

[25] Xiong C, Lu X, Lin X. Damage assessment of shear wall components for RC frame–shear wall buildings using story curvature as engineering demand parameter. Eng Struct 2019;189:77–88.

[26] Fritzen CP. Vibration-based structural health monitoring–concepts and applications. Key Eng Mater 2005;293:3–20.

[27] Montalvao D, Maia NMM, Ribeiro AMR. A review of vibration-based structural health monitoring with special emphasis on composite materials. Shock Vib Dig 2006;38(4):295–324.

[28] Nagarajaiah S, Dyke S, Lynch JP, Smyth A, Agrawal A, Symans M, Johnson E. Current directions of structural health monitoring and control in USA. Adv Sci Technol 2009;56:277–86.

[29] Das S, Saha P, Patro S. Vibration-based damage detection techniques used for health monitoring of structures: a review. J Civ Struct Heal Monit 2016;6:477–507.

[30] Hu H, Tang M, Li L, Hu H, Qiao S. Signal processing techniques for structural health monitoring of super high-rise buildings. In: IOP conference series: earth and environmental science. vol. 330, IOP Publishing; 2019, 022015.

[31] Amezquita-Sanchez JP, Adeli H. Signal processing techniques for vibration-based health monitoring of smart structures. Arch Comput Methods Eng 2016;23:1–15.

[32] Caesarendra W, Tjahjowidodo T. A review of feature extraction methods in vibration-based condition monitoring and its application for degradation trend estimation of low-speed slew bearing. Mach 2017;5(4):21.

[33] Tronci E, De Angelis M, Betti R, Altomare V. Vibration-based structural health monitoring of a RC-masonry tower equipped with non-conventional TMD. Eng Struct 2020;224:111212.

[34] Javadinasab Hormozabad S, Gutierrez Soto M, Adeli H. Integrating structural control, health monitoring, and energy harvesting for smart cities. Expert Syst 2021;38(8):e12845.

[35] Roy K, Ray-Chaudhuri S. Fundamental mode shape and its derivatives in structural damage localization. J Sound Vib 2013;332(21):5584–93.

[36] Zhang F-L, Ventura CE, Xiong H-B, Lu W-S, Pan Y-X, Cao J-X. Evaluation of the dynamic characteristics of a super tall building using data from ambient vibration and shake table tests by a Bayesian approach. Struct Control Heal Monit 2018;25(4):e2121.

[37] Michel C, Gueguen P. Time-frequency analysis of small frequency variations in civil engineering structures under weak and strong motions using a reassignment method. Struct Heal Monit 2010;9(2):159–71.

[38] Amezquita-Sanchez JP, Adeli H. Synchrosqueezed wavelet transform-fractality model for locating, detecting, and quantifying damage in smart highrise building structures. Smart Mater Struct 2015;24(6):065034.

[39] Bahar O, Ramezani S. Enhanced Hilbert–Huang transform and its application to modal identification. Struct Des Tall Spec Build 2014;23(4):239–53.

[40] Shabbir F, Omenzetter P. Particle swarm optimization with sequential niche technique for dynamic finite element model updating. Comput- Aided Civ Infrastruct Eng 2015;30(5):359–75.

[41] Zhang F-L, Yang Y-P, Xiong H-B, Yang J-H, Yu Z. Structural health monitoring of a 250-m super-tall building and operational modal analysis using the fast Bayesian FFT method. Struct Control Heal Monit 2019;26(8):e2383.

[42] Valdés-González J, De-la Colina J, González-Pérez CA. Experiments for seismic damage detection of a RC frame using ambient and forced vibration records. Struct Control Heal Monit 2015;22(2):330–46.

[43] Gkoktsi K, Giaralis A. A compressive MUSIC spectral approach for identification of closely-spaced structural natural frequencies and post-earthquake damage detection. Probabilistic Eng Mech 2020;60:103030.

[44] Makki Alamdari M, Anaissi A, Khoa NL, Mustapha S. Frequency domain decomposition-based multisensor data fusion for assessment of progressive damage in structures. Struct Control Heal Monit 2019;26(2):e2299.

[45] Bursi* OS, Kumar A, Abbiati G, Ceravolo R. Identification, model updating, and validation of a steel twin deck curved cable-stayed footbridge. Comput- Aided Civ Infrastruct Eng 2014;29(9):703–22.

[46] Kaveh A, Zolghadr A. An improved CSS for damage detection of truss structures using changes in natural frequencies and mode shapes. Adv Eng Softw 2015;80:93–100.

[47] Zhang C, Mousavi AA, Masri SF, Gholipour G, Yan K, Li X. Vibration feature extraction using signal processing techniques for structural health monitoring: A review. Mech Syst Signal Process 2022;177:109175.

[48] Worden K, Farrar CR, Manson G, Park G. The fundamental axioms of structural health monitoring. Proc R Soc A: Math Phys Eng Sci 2007;463(2082):1639–64.

[49] Simoen E, De Roeck G, Lombaert G. Dealing with uncertainty in model updating for damage assessment: A review. Mech Syst Signal Process 2015;56:123–49.

[50] Lin Y-z, Nie Z-h, Ma H-w. Dynamics-based cross-domain structural damage detection through deep transfer learning. Comput- Aided Civ Infrastruct Eng 2022;37(1):24–54.

[51] Shumway RH, Stoffer DS, Stoffer DS. Time series analysis and its applications, vol. 3, Springer; 2000.

[52] Mei L, Li H, Zhou Y, Li D, Long W, Xing F. Output-only damage detection of shear building structures using an autoregressive model-enhanced optimal subpattern assignment metric. Sens 2020;20(7):2050.

[53] Kordestani H, Xiang Y-Q, Ye X-W. Output-only damage detection of steel beam using moving average filter. Shock Vib 2018;2018(1):2067680.

[54] Shi H, Worden K, Cross EJ. A cointegration approach for heteroscedastic data based on a time series decomposition: an application to structural health monitoring. Mech Syst Signal Process 2019;120:16–31.

[55] Okasha NM, Frangopol DM, Saydam D, Salvino LW. Reliability analysis and damage detection in high-speed naval craft based on structural health monitoring data. Struct Heal Monit 2011;10(4):361–79. http://dx.doi.org/10.1177/1475921710379516.
[56] Tatsis K, Dertimanis V, Ou Y, Chatzi E. GP-ARX-based structural damage detection and localization under varying environmental conditions. J Sens Actuator Netw 2020;9(3):41.
[57] Modesto AJ, Birgul R, Werlink RJ, Catbas FN. Damage detection of composite overwrapped pressure vessels using ARX models. Int J Press Vessels Pip 2021;192:104410.
[58] Markogiannaki O, Arailopoulos A, Giagopoulos D, Papadimitriou C. Vibration-based damage localization and quantification framework of large-scale truss structures. Struct Heal Monit 2023;22(2):1376–98.
[59] Gul M, Catbas FN. Structural health monitoring and damage assessment using a novel time series analysis methodology with sensor clustering. J Sound Vib 2011;330(6):1196–210. http://dx.doi.org/10.1016/j.jsv.2010.09.024, URL https://www.sciencedirect.com/science/article/pii/S0022460X10006292.
[60] Do NT, Gül M. Structural damage detection under multiple stiffness and mass changes using time series models and adaptive zero-phase component analysis. Struct Control Heal Monit 2020;27(8):e2577.
[61] Yu H, Zhu H, Weng S, Wen W, Yan A, Yu X. Substructural damage identification using autoregressive moving average with exogenous inputs model and sparse regularization. Adv Struct Eng 2023;26(9):1621–35.
[62] Daneshvar MH, Gharighoran A, Zareei SA, Karamodin A. Early damage detection under massive data via innovative hybrid methods: application to a large-scale cable-stayed bridge. Struct Infrastruct Eng 2021;17(7):902–20.
[63] Kopsaftopoulos F, Fassois S. A functional model based statistical time series method for vibration based damage detection, localization, and magnitude estimation. Mech Syst Signal Process 2013;39(1):143–61. http://dx.doi.org/10.1016/j.ymssp.2012.08.023, URL https://www.sciencedirect.com/science/article/pii/S0888327012003536.
[64] Entezami A, et al. Structural health monitoring by time series analysis and statistical distance measures. Springer; 2021.
[65] Avendaño-Valencia L, Fassois S. Stationary and non-stationary random vibration modelling and analysis for an operating wind turbine. Mech Syst Signal Process 2014;47(1–2):263–85.
[66] Poulimenos AG, Fassois SD. Output-only stochastic identification of a time-varying structure via functional series TARMA models. Mech Syst Signal Process 2009;23(4):1180–204.
[67] Chen J, Jiang X, Yan Y, Lang Q, Wang H, Ai Q. Dynamic warning method for structural health monitoring data based on ARIMA: Case study of Hong Kong–Zhuhai–Macao bridge immersed tunnel. Sens 2022;22(16):6185.
[68] Buckley T, Pakrashi V, Ghosh B. A dynamic harmonic regression approach for bridge structural health monitoring. Struct Heal Monit 2021;20(6):3150–81.
[69] Bruggi M, Mariani S. Optimization of sensor placement to detect damage in flexible plates. Eng Optim 2013;45(6):659–76.
[70] Capellari G, Chatzi E, Mariani S. Optimal sensor placement through Bayesian experimental design: Effect of measurement noise and number of sensors. In: Proceedings. vol. 1, MDPI; 2016, p. 41.
[71] Capellari G, Chatzi E, Mariani S. Cost-benefit optimization of sensor networks for SHM applications. In: Proceedings. vol. 2, MDPI; 2017, p. 132.
[72] Chun P-j, Yamashita H, Furukawa S. Bridge damage severity quantification using multipoint acceleration measurement and artificial neural networks. Shock Vib 2015;2015(1):789384.
[73] Rafiei MH, Adeli H. A novel unsupervised deep learning model for global and local health condition assessment of structures. Eng Struct 2018;156:598–607.
[74] Ma X, Lin Y, Nie Z, Ma H. Structural damage identification based on unsupervised feature-extraction via variational auto-encoder. Meas 2020;160:107811.
[75] Azimi M, Pekcan G. Structural health monitoring using extremely compressed data through deep learning. Comput- Aided Civ Infrastruct Eng 2020;35(6):597–614.
[76] Xu S, Noh HY. Knowledge transfer between buildings for seismic damage diagnosis through adversarial learning. 2020, arXiv preprint arXiv:2002.09513.
[77] Bao N, Zhang T, Huang R, Biswal S, Su J, Wang Y. A deep transfer learning network for structural condition identification with Limited Real-World Training Data. Struct Control Heal Monit 2023;2023(1):8899806.
[78] Lin Y-z, Nie Z-h, Ma H-w. Structural damage detection with automatic feature-extraction through deep learning. Comput- Aided Civ Infrastruct Eng 2017;32(12):1025–46.
[79] Zhang Y, Miyamori Y, Mikami S, Saito T. Vibration-based structural state identification by a 1-dimensional convolutional neural network. Comput- Aided Civ Infrastruct Eng 2019;34(9):822–39.
[80] Chang C-M, Lin T-K, Chang C-W. Applications of neural network models for structural health monitoring based on derived modal properties. Meas 2018;129:457–70.
[81] Peng J, Zhang S, Peng D, Liang K. Application of machine learning method in bridge health monitoring. In: 2017 second international conference on reliability systems engineering. ICRSE, IEEE; 2017, p. 1–7.
[82] Liang X. Image-based post-disaster inspection of reinforced concrete bridge systems using deep learning with Bayesian optimization. Comput- Aided Civ Infrastruct Eng 2019;34(5):415–30.
[83] Li X, Xi H, Zhou C, Gu W, Gao T. Damage degree identification of crane girder based on the support vector machine. In: 2018 prognostics and system health management conference (PHM-chongqing). IEEE; 2018, p. 920–4.
[84] Chun P-j, Yamane T, Izumi S, Kuramoto N. Development of a machine learning-based damage identification method using multi-point simultaneous acceleration measurement results. Sens 2020;20(10):2780.
[85] Sun L, Shang Z, Xia Y, Bhowmick S, Nagarajaiah S. Review of bridge structural health monitoring aided by big data and artificial intelligence: From condition assessment to damage detection. J Struct Eng 2020;146(5):04020073.
[86] Flah M, Nunez I, Ben Chaabene W, Nehdi ML. Machine learning algorithms in civil structural health monitoring: A systematic review. Arch Comput Methods Eng 2021;28(4):2621–43.
[87] Mishra M. Machine learning techniques for structural health monitoring of heritage buildings: A state-of-the-art review and case studies. J Cult Herit 2021;47:227–45.
[88] Ancheta TD, Darragh RB, Stewart JP, Seyhan E, Silva WJ, Chiou BS-J, Wooddell KE, Graves RW, Kottke AR, Boore DM, et al. NGA-West2 database. Earthq Spectra 2014;30(3):989–1005.
[89] Lu Y, Henry R, Zhou Y, Rodgers G, Yang Q, Gu A, Elwood K, Yang T. Shake table test of a 2-storey low-damage concrete wall building. Designsafe- CI 2021. http://dx.doi.org/10.17603/DS2-NCAC-SG36.